JOURNAL OF MATERIALS SCIENCE 27 (1992) 2557–2579

Review
Supermolecular structure of isotactic polypropylene

J. VARGA
Department for Plastics and Rubber Industry, Faculty of Chemical Engineering, Budapest Polytechnical University, H-1111 Budapest, Hungary

The crystalline structure, spherulitic crystallization and melting behaviour of isotactic polypropylene (iPP) is comprehensively reviewed, illustrated and discussed. It is demonstrated and summarized how the nucleation, development and growth of the different spherulites depend on the crystallization and melting conditions both in quiescent and sheared melt. Based on the results the microtexture development during real processing conditions is elucidated for selected examples. Several subjects of intense debate on the above topics are clarified using evidence from polarized optical micrography and differential scanning calorimetry.

1. Introduction

During the crystallization of polymers, various supermolecular structures form as aggregates of chain-folded fibrillar or lamellar primary crystallites with definite geometrical arrangements. When polymers crystallize in a melt, different supermolecular formations may develop [1–3], most frequently spherulites and cylindrites (axialites), with some hedrites (polygonal formations), quadrites (tetragonal formations), and dendrites (pine-shaped formations). Supermolecular structures may be readily visualized by polarizing optical microscopy while their constituents, the primary crystallites, may usually be observed only by electron microscopy. The characteristics of supermolecular structure are markedly influenced by the thermal conditions, mechanical effects, and by the presence of extraneous materials.

In the present review, essential results from the polarizing optical microscopy of the supermolecular structure of isotactic polypropylene (iPP) are surveyed.

2. Crystalline structure of iPP

iPP was the first representative of the industrially manufactured stereoregular polymers. It has a high tendency to crystallize [4]. iPP is a polymorphic material with a number of crystal modifications [5], such as monoclinic (α), hexagonal (β), and triclinic (γ). The monoclinic (α), modification occurs most frequently [6–8]. In the crystallization of conventional iPP grades, essentially the α-modification is formed which may be accompanied by a lower or higher amount of β-modification at higher undercooling [9]. Under special crystallization conditions, however, when the "temperature gradient method" [10–12] is used or when selective β-nucleating agents are present, the product will be quite rich in β-modifications [13–29]. Varga *et al.* [30–33] prepared the pure β-modification in the presence of selective β-nucleating agents, by the appropriate selection of the thermal conditions of crystallization. The γ-modification may form in degraded, low molecular weight PP or in samples crystallized under high pressure [5, 25, 34–42]. Quenching (abrupt cooling) the molten polymer leads to an intermediate crystalline order, indicated by two diffuse X-ray diffraction peaks, which is different from both the crystalline and the amorphous states. The interpretation of the structure formed is still disputed in the literature [43–48].

Consequently, iPP can comprise a variety of supermolecular structures implying crystallites of different modifications. The formation of supermolecular structures of α- and β-modifications of iPP was first demonstrated by Padden and Keith [9].

3. Spherulitic crystallization of iPP

Spherulitic structure generally appears when crystallization is conducted in the viscous state and/or at a high undercooling [1–3]. Polymers in a quiescent melt crystallize essentially into spherulitic structures. Following crystallization in a thin film of melt (two-dimensional crystallization), transmission optical microscope between crossed polarizers reveals the development of birefringent disc-like formations on randomly formed crystal nuclei, growing radially at a constant rate (linear growth rate) under isothermal conditions. When they come into contact with each other, the growth fronts of the spherulites finally result in a multitude of polygonal formations confined by straight or curved lines (Fig. 1).

The term "spherulite" indicates an aggregate of primary crystallites of spherical shape or spherical

0022–2461

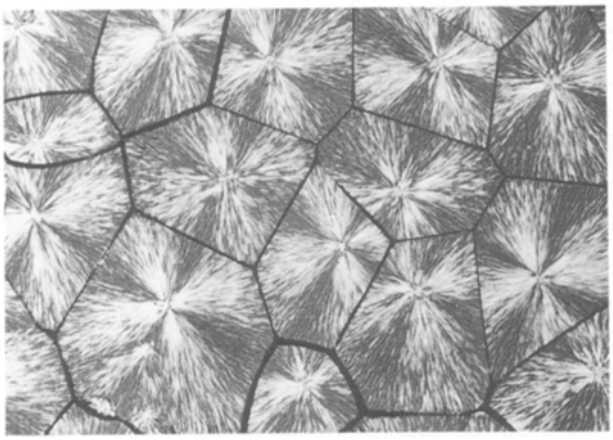

Figure 1 Sample consisting of negative radial α-spherulites (α_{II}); $T_c = 413$ K.

symmetry consisting of crystallites growing from a central nucleus uniformly in all steric directions. Complete filling of the space is provided by further branching of fibrils from the main growth of fibrils at small non-crystallographic angles. Spherulites can be considered to be radially symmetrical, optically uniaxial crystals. Consequently, the polarizing microscopic pattern of a spherulite show a central dark cross (Maltese cross) with wings coincident with the respective planes of polarizer and analyser. The phenomenological theory of spherulitic crystallization of polymers was developed by Keith and Padden [49, 50]. According to these authors, the contaminating components (e.g. fractions with low, if any, tendency to crystallize), segregated from the melt in the vicinity of the crystallization front, are responsible for the branching of the fibrils. Bassett and Vaughan [51], however, drew attention to some contradictions in this phenomenological theory based on electron microscopic studies on spherulites.

Nuclei inducing the formation of spherulites are pin-point type (at least on the resolution of optical microscopy) or fibril type. In the latter case, primary crystallites growing and branching from the nucleus may transform into the characteristic radially symmetric form of spherulites through transient sheaf-like or oval formations [52, 53]. In this case, in contrast to the spherulite as a whole, no spherical symmetry exists in the vicinity of the centre of the spherulite. This non-homogeneous central region in α- and β-spherulites of iPP was demonstrated experimentally [53–55]. In fact, the process of spherulite nucleation [56], and the sheaf-like nucleation sites were also discovered. Herdt and Kallweit [57] analysed the possible types of supermolecular aggregates of fibrils growing from a fibrillar nucleus through several branches at different angles and frequencies. They conducted a computerized simulation for their possible formation and compared them to the real ones. The formation of a transient sheaf-like structure from a fibrillar nucleus and its further transformation into the spherical symmetry of spherulites were analysed quantitatively by Dobbert [58] who also clarified the effect of this process on the time dependence of the overall crystallization.

Using polarizing optical microscopy, several characteristic types of spherulite can be distinguished (Figs 1–5). Depending on the feature of fibrils, the spherulites can be radial or ringed type. In radial spherulites, the fibrils are straight while, in the ringed ones, they are helical, i.e. twisted around their longitudinal axes [2]. Consequently, in the polarizing micrographs, concentric dark rings appear corresponding to the pitch of the helix (Fig. 5). Depending

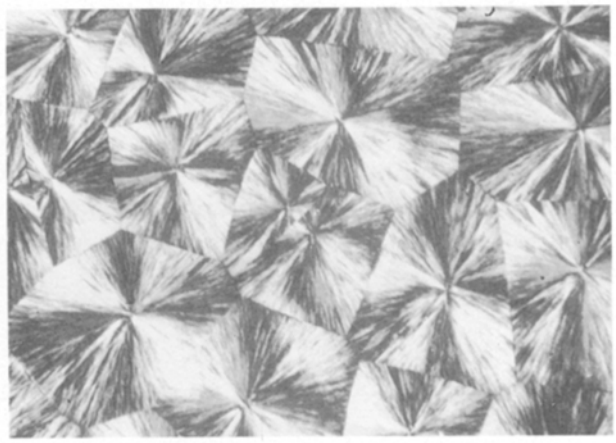

Figure 2 Sample consisting of positive radial α-spherulites (α_I); $T_c = 393$ K.

Figure 3 Sample consisting of mixed radial α-spherulites (α_m); $T_c = 403$ K.

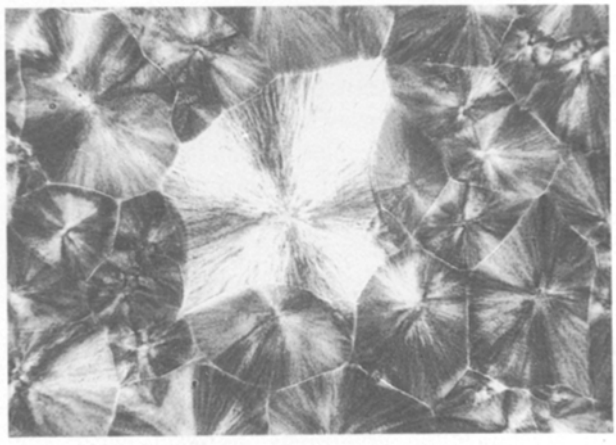

Figure 4 Negative radial β-spherulite (β_{III}) in the field of α-spherulites; $T_c = 393$ K.

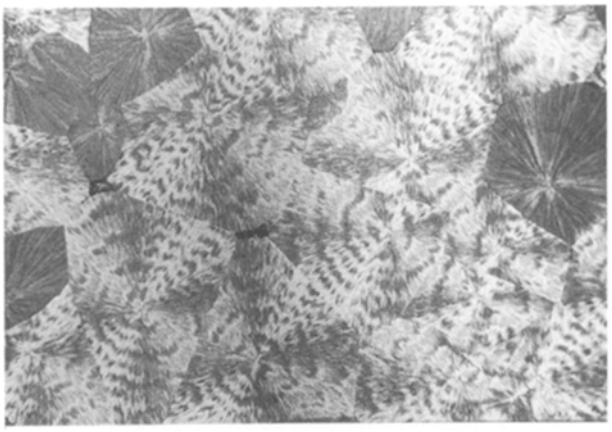

Figure 5 Sample comprising negative ringed β-spherulites (β_{IV}); $T_c = 408$ K.

on the birefringence, spherulites can be optically positive or negative [3]. The birefringence of a spherulite, Δn, is defined as

$$\Delta n = n_r - n_t \quad (1)$$

where n_r, n_t are the refractive indices along the radial and tangential direction of the spherulite, respectively. Consequently, in the case of positive spherulite, n_r is greater than n_t and, for the negative one, n_r smaller than n_t. The optical character, i.e. the sign of birefringence of the spherulites can be determined by means of a primary red filter (λ-plate) located diagonally between crossed polarizers. In this way the first and third quarter of the sight are blue and the second and fourth ones are yellow (Fig. 2) when the spherulites are positive, while a reversed arrangement of the quarters is observed (Fig. 1) for negative spherulites. (For a more detailed review, see [59].) It should be noted that the black-and-white copies of coloured pictures are presented here representing the yellow and blue fields by lighter and darker tints, respectively.

Padden and Keith [9] were the first to report five different types of spherulites consisting of α- and β-modifications (α- and β-spherulites formed during the melt crystallization of iPP). They demonstrated that three types of α-spherulite might be formed depending on the temperature of crystallization: positive radial (marked I) below 407 K, negative radial above 410 K (marked II), and mixed-type spherulites in the intermediate range (Figs 1–3). The latter has no inevitable optical character and shows no Maltese cross in the micrograph (Fig. 3).

Two types of β-spherulite were detected to form sporadically with the α-modification [9]: negative radial (marked III), highly birefringent, below 401 K, and negative ringed (marked IV) between 401 and 405 K (Figs 4 and 5). Padden and Keith [9] marked the various types of spherulites with Roman numerals. The present report departs from this notation, using α_I, α_{II}, α_m as well as β_{III} and β_{IV}, which indicate the modification, and the subscripts refer to the notations of Padden and Keith [60]. The observations of Padden and Keith [9] were essentially supported by subsequent investigations, but the temperature ranges for the formation of the particular types of spherulites have been corrected more or less, presumably due to the variability in the characteristics of the molecular structure of iPP types studied [53, 61].

In Varga's comprehensive studies [30, 33, 60], the temperature ranges of the formation of PP β-modification (β-PP) were rendered more reliable. He demonstrated that the formation of β-PP had a theoretical upper temperature limit ($T_{\beta\alpha} = 413$–414 K), while indirect experimental data [30] referred to a possible lower temperature limit ($T_{\alpha\beta} \approx 373$ K). Recently, the existence of $T_{\alpha\beta}$ was proved by direct experiments [62].

Later, formation of some new types of spherulite was also detected.

With a high-temperature crystallization of iPP ($T_c = 420$–430 K), Awaya [63] observed several new types of α-spherulites, designated pseudo-positive, pseudo-negative, neo-mixed, high-temperature positive, and flower-like ones. In our laboratory, highly degraded iPP produced positive α-spherulites (Fig. 6) independently of the crystallization temperature where monofibrils and small-angle branches of fibrils became visible even by optical microscopy. During a self-seeded high-temperature crystallization ($T_c = 423$–433 K), positive α-spherulites were found [55, 56] in contrast to the observations of Padden and Keith [9]. In our own experiments, the random appearance of hexagonal hedrites of β-modification was detected in addition to the α-spherulites even at a low-resolution optical level (Fig. 7). At a further stage of growth, they eventually transformed into a radial symmetry characteristic of the spherulitic structure. Using electron microscopy, Geil [64] and Olley [65] detected β-hedrites produced by melt crystallization. The micrographs suggest that hedrites are derived from a spiral growth of lamellae round a screw dislocation. The size of the hedrites is about 1 μm [65].

The formation of spherulites of positive and mixed optical character is unexpected in polymers. According to the structural model based on the radial growth and small-angle branching of fibrils, the molecular chains folded into fibrils are nearly or exactly perpendicular to the radius of the spherulites. As the refractive index is higher in the chain direction than perpendicularly, the primary fibrils have a negative

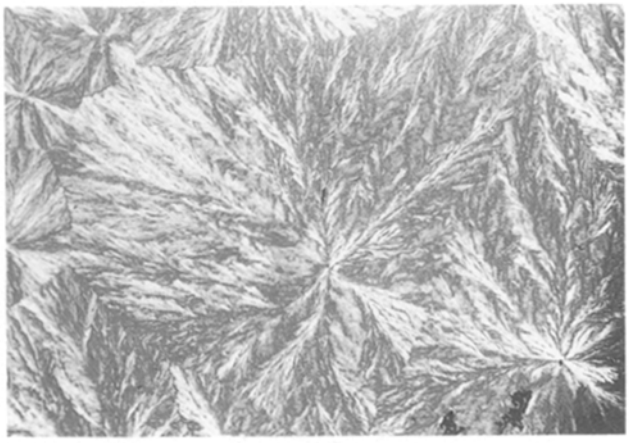

Figure 6 Positive α-spherulite formed in a degraded iPP sample with fibrillar structure resolved at the optical level.

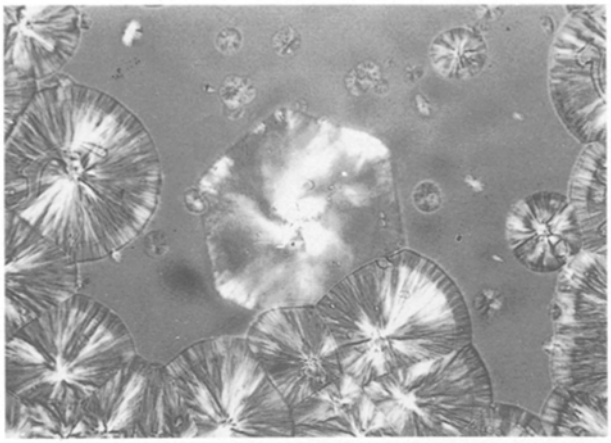

Figure 7 Hydrite (hexagonal formation) of β-modification in the field of α-spherulites.

optical character. Correspondingly, polymers are expected to produce only optically negative spherulites. The experimental results on the structure of positive and mixed spherulites in iPP were reviewed by Norton and Keller [53]. It was demonstrated unequivocally by electron microscopy that α-spherulites contained fibrils with large-angle branches even at about 80° to the radius of the spherulite [53, 54]. This was in good agreement with Khoury's data [66] for twin crystals grown by crystallization in solution and with other observations [67–71]. The structure of the positive and mixed spherulites was interpreted by the "cross-hatched" model [53–56, 72] where radial fibrils were accompanied by a great number of tangential ones. Assuming a quadratic arrangement of fibrils, the relative amount of radial and tangential fibrils in various types of α-spherulites was determined by Idrissi *et al.* [73] using optical microscopy, light scattering, and calorimetry.

The optical character of α-spherulites is controlled by the ratio of radial to tangential fibrils. Raising the temperature of crystallization leads to a reduction in the proportion of tangential ones [53] and, simultaneously, a positive to negative character transformation. No tangential fibrils form above 428 K [56]. It was also revealed [53] that the thickness of tangential fibrils was lower than that of the radial ones.

Structural and optical characteristics of β-spherulites were studied comprehensively by Samuels [74, 75]. He found intrinsic refractive indices in the hexagonal (β) modification of 1.536 and 1.506 in the *c*- (chain direction) and *a*-axis directions respectively, resulting in a strong negative optical character. He also revealed that the tangential refractive index of β_{III}-spherulites was constant (1.507) while it changed periodically between 1.496 and 1.519 in β_{IV}-spherulites according to their ringed feature.

The arrangement of the fibrils in β-spherulites is radial, as is usual in polymeric spherulites, and no traces of cross-hatched structure can be detected [53]. The central region of β-spherulites comprises non-homogeneous and sheaf-like branched fibrils [53].

3.1. Melting of spherulites

The melting characteristics of iPP spherulites were studied by Padden and Keith [9]. They established that positive and mixed α-spherulites gradually transformed into the negative type when warmed and melted. On the other hand, β-spherulites recrystallized into the α-modification during heating. This observation, supported by other authors [11–13, 16–18, 25, 28] has led to the assumption of thermodynamic instability of the β-modification.

Subsequently, Varga [30] pointed out that melting of the β-modification had a specific feature including a much more complicated process than that outlined above. Namely, the melting characteristics of β-PP are highly dependent on the thermal post history of the crystalline sample. In other words, a melting memory effect takes place. In contrast to the current concept in the literature [9, 11–13, 16–18, 25, 28], when heating begins from the temperature of crystallization, the β-modification does not recrystallize into the α-form. Instead, they melt separately, like the thermodynamically stable modifications. However, if samples containing β-PP are cooled below a critical temperature, T_R^*, before heating, the partial melting is accompanied by a recrystallization into α-form (βα-recrystallization) and, finally, they melt in the α-form. This critical recooling temperature, T_R^*, is ~ 373–383 K [30–33]. Consequently, a βα-recrystallization susceptibility appears due to recooling.

An optical representation of the melting memory effect is shown in Figs 8 and 9, in samples containing radial negative α-spherulites and ringed negative β-spherulites after the isothermal crystallization at $T_c = 408$ K. The separate melting of β-spherulites is presented in Fig. 8, while βα-recrystallization of β-spherulites in recooled samples during the partial melting is seen in Fig. 9 where negative ringed β-spherulites transform into positive ringed -α-spherulites preserving the ringed character up to complete melting. The α-modification recrystallized from β-spherulites has a higher melting point than α-spherulites originally present in the sample formed isothermally (Fig. 9c). The higher melting point of the α-modification formed by recrystallization is thought to be due to its higher (re)crystallization temperature. The appearance of the tendency to βα-recrystallization of β-PP cooled below T_R^* can be attributed to the formation of an α-phase within the spherulites in the temperature range below T_R^*, due to a secondary crystallization taking place in the cooling process. This phase acts as an α-nucleating agent during the partial melting of β-spherulites [30]. Presumably, the lower limit temperature of β-PP formation, $T_{\alpha\beta}$, is in the vicinity of T_R^*.

It should be noted that the experimental melting point of spherulites (the temperature of the complete disappearance of birefringence) depends on the temperature or temperature range of crystallization; thus, it cannot be considered to be a material constant. In a sample subjected to the usual crystallization conditions, the melting points of the α- and β-modifications are ~ 440 and ~ 425 K, respectively. The thermodynamic equilibrium melting point, T_m^0, i.e. the melting

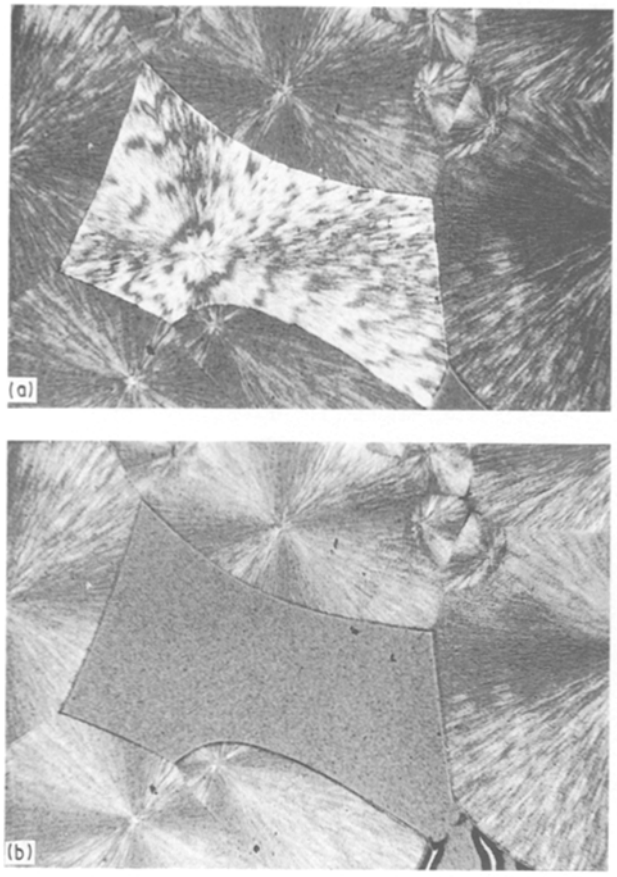

Figure 8 Separate melting of ringed β-spherulites. Heating was started from T_c (T_c = 410 K), (a) The original sample (T_c = 410 K). (b) T = 433 K during heating ($T < T_m/\alpha/$).

temperature of a perfect crystal of infinite size, determined by various extrapolation methods, is an important real material constant. The following relation can be established between the experimental, T_m, and the thermodynamic equilibrium melting points, T_m^0 [76]

$$T_m = T_m^0\left(1 - \frac{2\sigma}{L\Delta H_f}\right) \qquad (2)$$

where L is the thickness of the folded-chain crystallites, σ the folded surface energy of crystallites, and ΔH_f is the heat of fusion. L increases with increasing T_c; consequently, T_m also increases simultaneously. Literature data for T_m^0 of the α- and β-modifications are highly contradictory. For T_m^0 of the α-modification, the folllowing values were reported: 449 K [77], 449.6 K [78], 451.4 K [79], 458 K [75, 80] 459 K [81, 82], 460.5 K [83], 481 K [84, 85], 485 K [86], and 493 K [75, 87]. For that of the β-modification the values given were: 443 K [74], 450 K [80], 457 K [33], 465 K [26], and 473 K [12]. The author accepts 457 ± 4 K as the most reliable T_m^0 of the β-modification [33] obtained with pure β-PP when the disturbance of βα-recrystallization was eliminated. Therefore, T_m^0 = 481 K is considered to be the most probable value for the α-modification [84, 85].

One feature of the spherulitic structure of iPP formed in isothermal or non-isothermal crystallization is

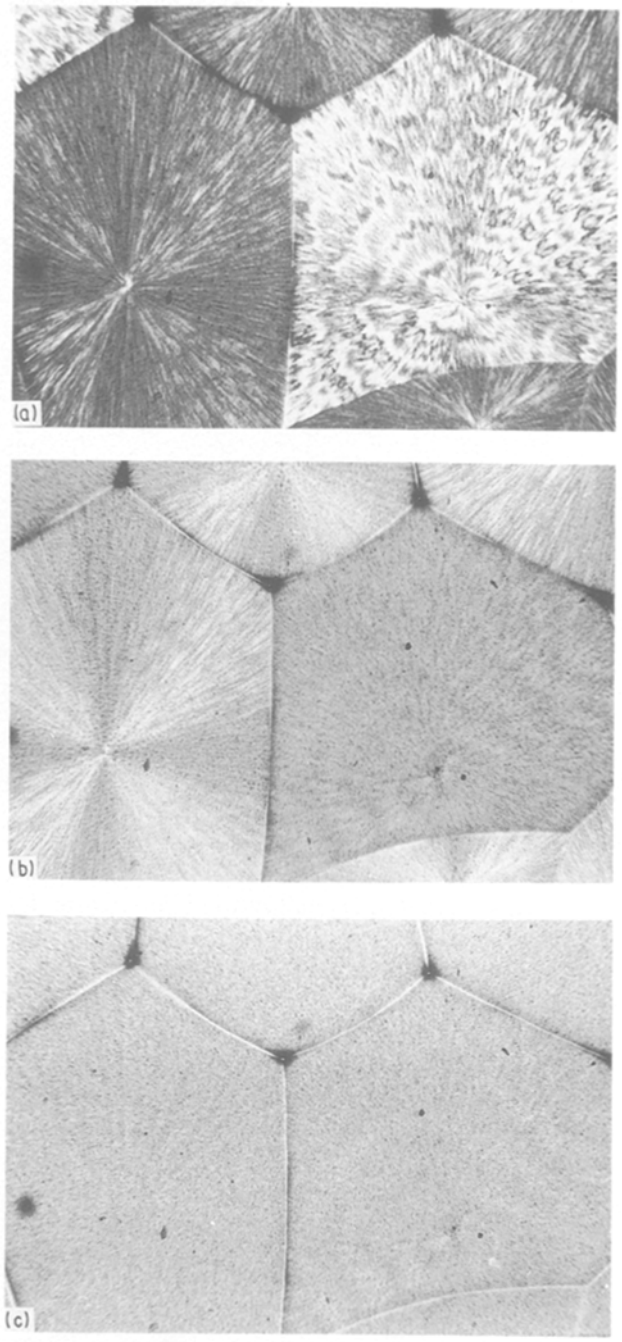

Figure 9 βα-recrystallization of the ringed β-spherulite during the heating process, preceded by cooling to room temperature. (a) Initial sample at room temperature, (b) during heating at 433 K, (c) after melting of the original α-spherulites at 438 K.

illustrated in Fig. 10. On the right-hand side of the figure, the temperature range of formation of α- and β-types of spherulites is presented. On the temperature axis, the approximate temperatures of changes in spherulite type (e.g. T/I – m) are marked. Limit temperatures for the development of smectic structure and the theoretical lower and upper temperature limits ($T_{\beta\alpha}$ and $T_{\alpha\beta}$) of the formation of the β-modification, are also indicated in Fig. 10. It can be concluded from the notations of the zone labelled "isothermal" what kind of structure would form in a crystallization process at a certain T_c. In the section labelled "non-isothermal", information about the structure expected at different cooling rates (indicated by the straight lines $T = f(t)$ with different slopes) is obtained. At a constant cooling rate, crystallization proceeds at a

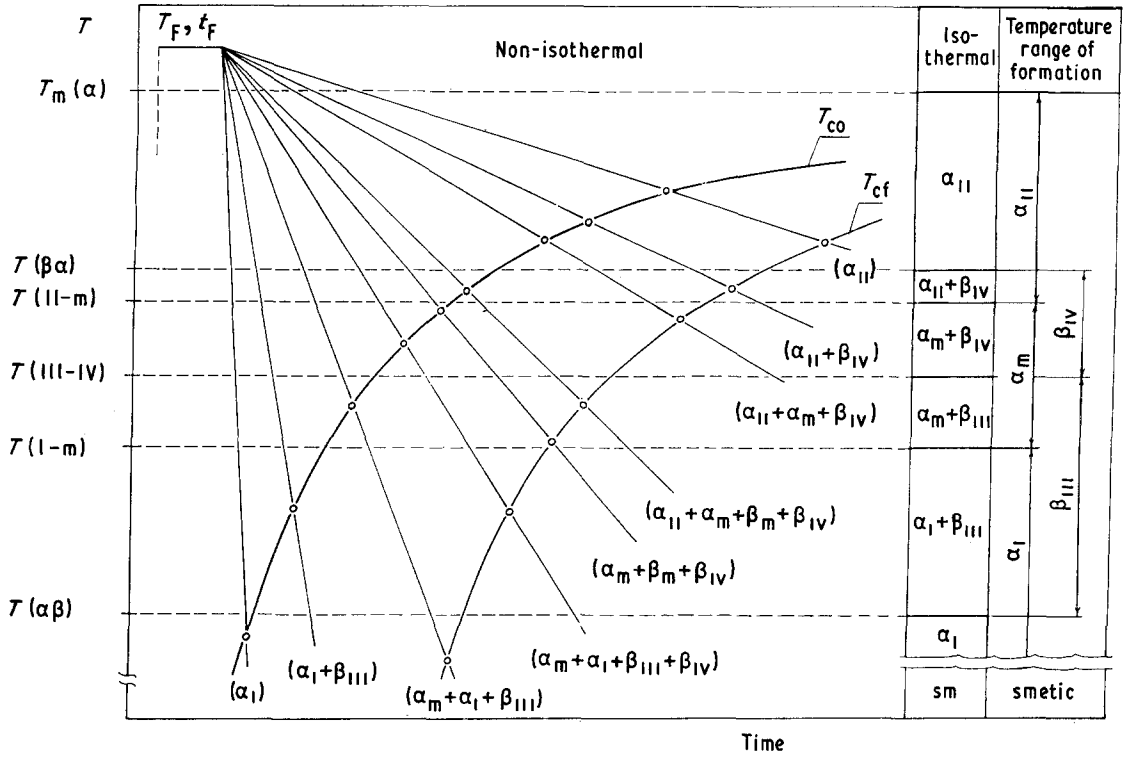

Figure 10 Formation of types of iPP spherulites during isothermal and nonisothermal crystallization.

continuously decreasing temperature from the initial, T_{c0}, to the final, T_{cf}, crystallization temperature. Increasing the cooling rate shifts T_{c0} and T_{cf} values towards the lower temperatures and the temperature range between them is widened. The temperature range of crystallization may, therefore, comprise the formation ranges of various types of spherulite depending on the cooling rate and thus, an extremely wide variety of structures can be produced. These are indicated in parentheses beside the individual cooling curves in Fig. 10. It should be emphasized that Fig. 10 is a schematic representation. The temperature ranges of crystallization may change for various iPP grades or in the presence of additives. Consequently, the features of the structure may also be altered.

It is worth mentioning that the optical character may vary even within a growing spherulite if the temperature is not constant during crystallization, as illustrated by the series of photographs in Fig. 11. The sample was crystallized in a two-step isothermal temperature regime where the crystallization temperature was periodically changed between 403 and 413 K. In this cyclic stepwise crystallization, α-spherulites consisting of mixed (α_m) and optically negative (α_{11}) annuli ("glorioles") are formed. The structure of the β-spherulites in the centre of the sample does not reflect any changes in T_c because, in the 403–413 K range, spherulites of β_{IV} type are produced (Fig. 11a).

A sample crystallized in two steps will melt in two steps (twice). Initially, the β-modification melts between 423 and 428 K beginning with its part formed at the lower temperature, followed by the other portion crystallized at the higher temperature (Fig. 11b, c). Then the α-modification melts in a similar two-step method between 438 and 443 K. It is clearly visible in the pictures by inspecting the colours in the quarters that the mixed spherulites transform into negative ones. The two-step melting of α- and β-spherulites is a descriptive optical representation of the general rule that the melting points of polymeric crystallites formed at higher T_c (i.e. having more equilibrated structure) are higher (cf. Equation 2). Step-wise melting was proved by calorimetry where separate melting peaks of α-crystallites formed at different temperatures could be unequivocally distinguished in the melting curves (Fig. 12). Because only traces of the β-modification were formed under these crystallization conditions, no peak for this modification was found in the melting curves.

The characteristics of the spherulitic crystallization of crystallizable block and random ethylene/propylene copolymers with low ethylene contents are somewhat different from those of iPP homopolymers. When commercial block copolymers are crystallized, the types of spherulite correspond to those observed by Padden and Keith [9]. Transformations during heating ($\alpha_I \rightarrow \alpha_m \rightarrow \alpha_{II}$ or $\alpha_m \rightarrow \alpha_{II}$) are also similar [88]. The spherulitic structure of block copolymers, however, has an essential feature which differs from that of homopolymers. On the surface of the spherulites, a fine distribution of drop-like heterogeneous inclusions appears. Their size depends on the ethylene comonomer content and on the crystallization conditions but its order of magnitude is about 1 μm. These drop-like inclusions become particularly discernible in the optical micrographs against the background of spherulites transformed into the optically negative form when heated to temperatures in the vicinity of the melting point (Fig. 13). The inclusions may be attributed to the phase separation of crystallized chain segments of ethylene sequences. This can also be proved by calorimetric measurements: around 380 K

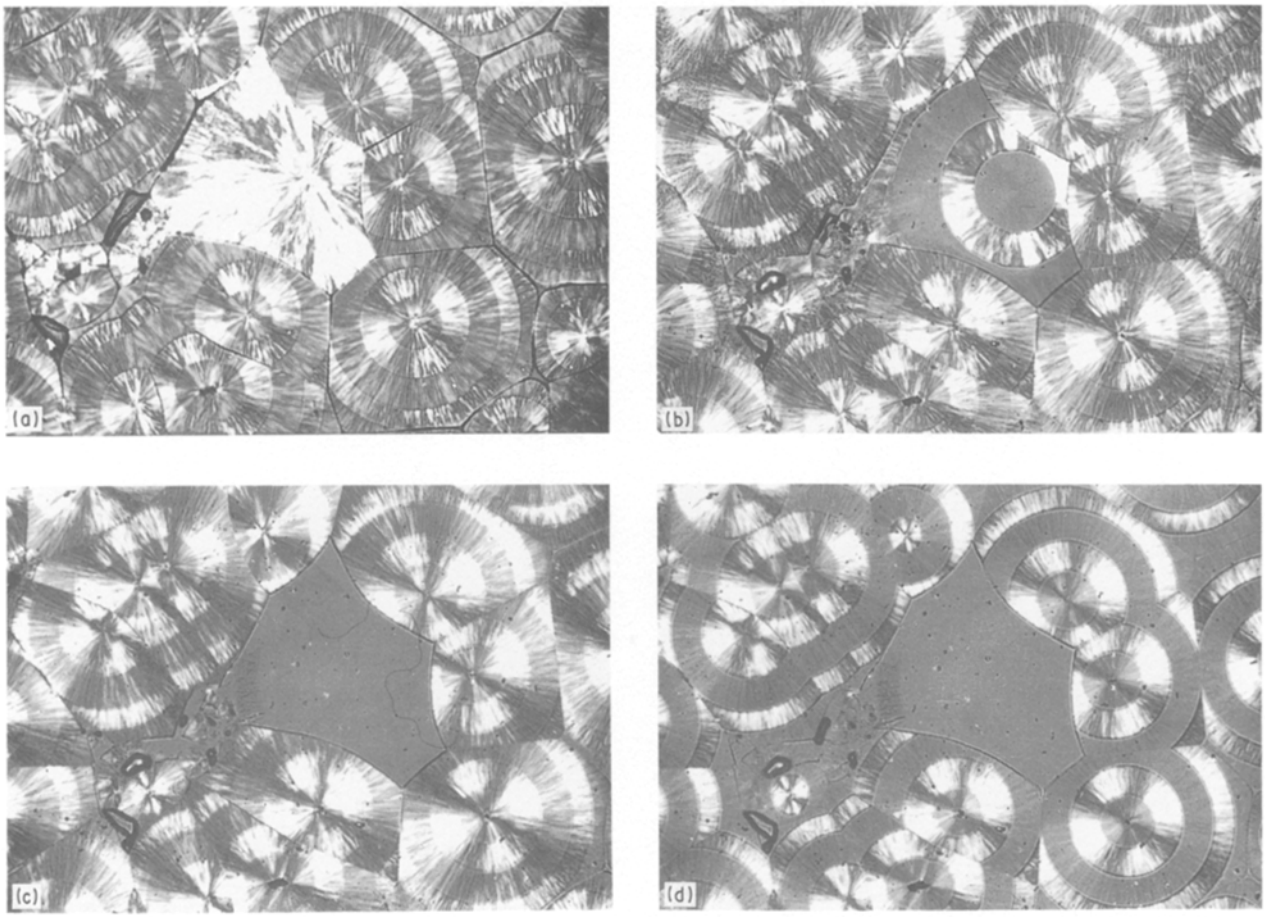

Figure 11 (a) Sample crystallized under cyclically alternating temperature steps (T_c = 403, 413 K) and (b–d) its stepwise melting. (a) Final stage of crystallization, (b) 425 K, (c) 433 K, (d) 440 K.

(the melting range of polyethylene), a diffuse endothermic peak appears in the melting curves of block copolymers. These observations make it probable that two separate crystalline phases are present in these block copolymers. Spherulitic structure and melting characteristics of block copolymers resemble those of polyethylene/polypropylene blends [89–91]. Prentice [92] used differential interference contrast microscopy to demonstrate the influence of producing technology (solvent or gas-phase process) on the heterogeneous phase structure of spherulites in block copolymers. He proved unequivocally that the gas phase process yielded real block copolymers instead of homopolymer blends. He found no phase separation in homopolymers, nor in random copolymers [92].

Copolymers with random ethylene distribution along the main chain are highly undercoolable polymers. For this reason, they crystallize into spherulitic structures, resolved readily at optical level, even at low temperatures. During the crystallization of a random copolymer, positive radial α-spherulites are formed together with traces of radial negative β-spherulites. The optical character of these α-spherulites, however, remains unchanged when heated; in fact, they melt in positive form. This behaviour, therefore, is different from that of type α_I spherulites of homopolymers and block copolymers produced by low-temperature crystallization [88].

The thermal conditions (crystallization temperature, cooling rate) of crystallization govern not only the type and optical character of spherulites, the polymorphic composition and the thermophysical characteristics (e.g. T_m) of the samples obtained, but also influence the size and size distribution of the spherulites. By reducing the crystallization temperature or by increasing the cooling rate (under otherwise unchanged conditions), the average spherulite size decreases due to an increase in the average density of nuclei. As a theoretical interpretation for the size reduction of spherulites with increasing undercooling ($\Delta T = T_m^0 - T_c$), the thermodynamic barrier of nucleation is proportional to ΔT^{-2} while that of growth is linear with ΔT^{-1} [93]. In other words, the rate of nucleation increases at a considerably greater extent than that of growth of nuclei when the temperature decreases.

In samples containing both modifications, β-spherulites are usually larger than α-spherulites. This can be attributed to the higher linear growth rate of β-spherulites [9]. Lovinger *et al.* [12] demonstrated that, in spite of the reduction in ratio between the growth rates of the two modifications (G_β/G_α) with increasing temperature, $G_\beta > G_\alpha$ consistently in the temperature range studied. Because β-spherulites form only below a certain temperature (405 K according to Padden and Keith [9]), no data are available in the literature

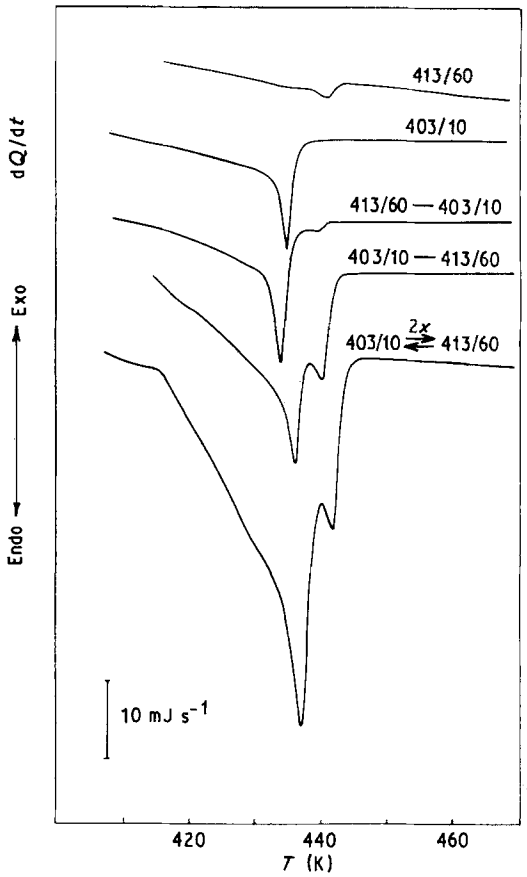

Figure 12 Calorimetric melting curves of iPP crystallized at two temperature levels ($T_c = 413$ K for $t_c = 60$ min, $T_c = 403$ K for $t_c = 10$ min) isothermally, at different sequences, and with cyclically alternating temperatures.

Figure 13 Spherulitic structure of a propylene block copolymer (Moplen EP-H 31 RA) after annealing.

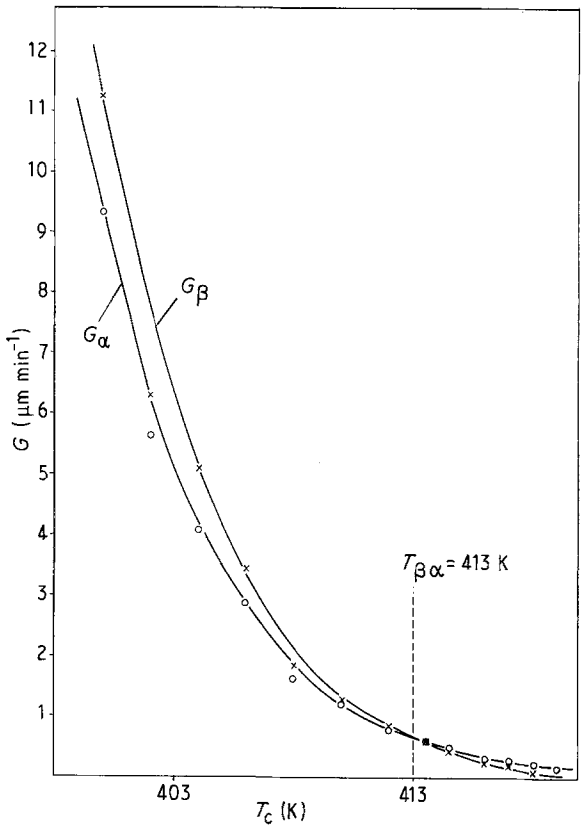

Figure 14 Temperature dependence of the linear growth rates (G_α, G_β) of α- and β-modifications.

for G_β in higher temperature ranges. Using the step-wise isothermal crystallization, the temperature range of G_β determination can be widened [60, 94]. With this method, β-spherulites are produced at a lower-temperature step followed by the measurement of the rate of continued growth at different higher temperatures.

The results from step-wise crystallization may be summarized as follows [94].

1. With increasing crystallization temperature, G_β/G_α decreasing and, above a certain temperature, $T_{\beta\alpha}$, in contrast to earlier literary data [9, 12], the growth rate of the α-modification exceeds that of the β-modifications. The level of $T_{\beta\alpha}$ is 413–414 K, as seen in Fig. 14.

2. If the second temperature step is higher than $T_{\beta\alpha}$, α-nuclei are formed on the surface of growing β-spherulites, developing α-spherulitic segments which finally overgrow the basic spherulite completely. This βα-bifurcation of growth during the step-wise crystallization and melting of this product is illustrated by the series of micrographs in Fig. 15. In the sample crystallized in two steps, regions of α- and β-modifications also melt in two steps. The shape of the α-segments on the surface of the growing β-spherulites is particularly conspicuous as the β-modifications have completely fused. It can be seen (at this stage) that they have developed from punctiform nuclei. Further, it can be deduced from the melting features that α-nuclei do not induce βα-recrystallization of the basic β-spherulites formed in the first step; moreover, β-spherulites continue to grow wherever they remain uncovered by α-segments, which enables the determination of G_β values even above $T_{\beta\alpha}$. This observation also proves that no βα-recrystallization is possible in the solid phase. There is a structural reason for this, namely, the elementary cells of the α-modification are packed with alternating clockwise and counter-clockwise helical chains, while the β-modification contains only unidirectional helices [14]. For a βα-recrystallization, therefore, rewinding of chains is required which is hindered in the solid phase.

3. The frequency of βα-bifurcation increases with the temperature of the second step, as illustrated by

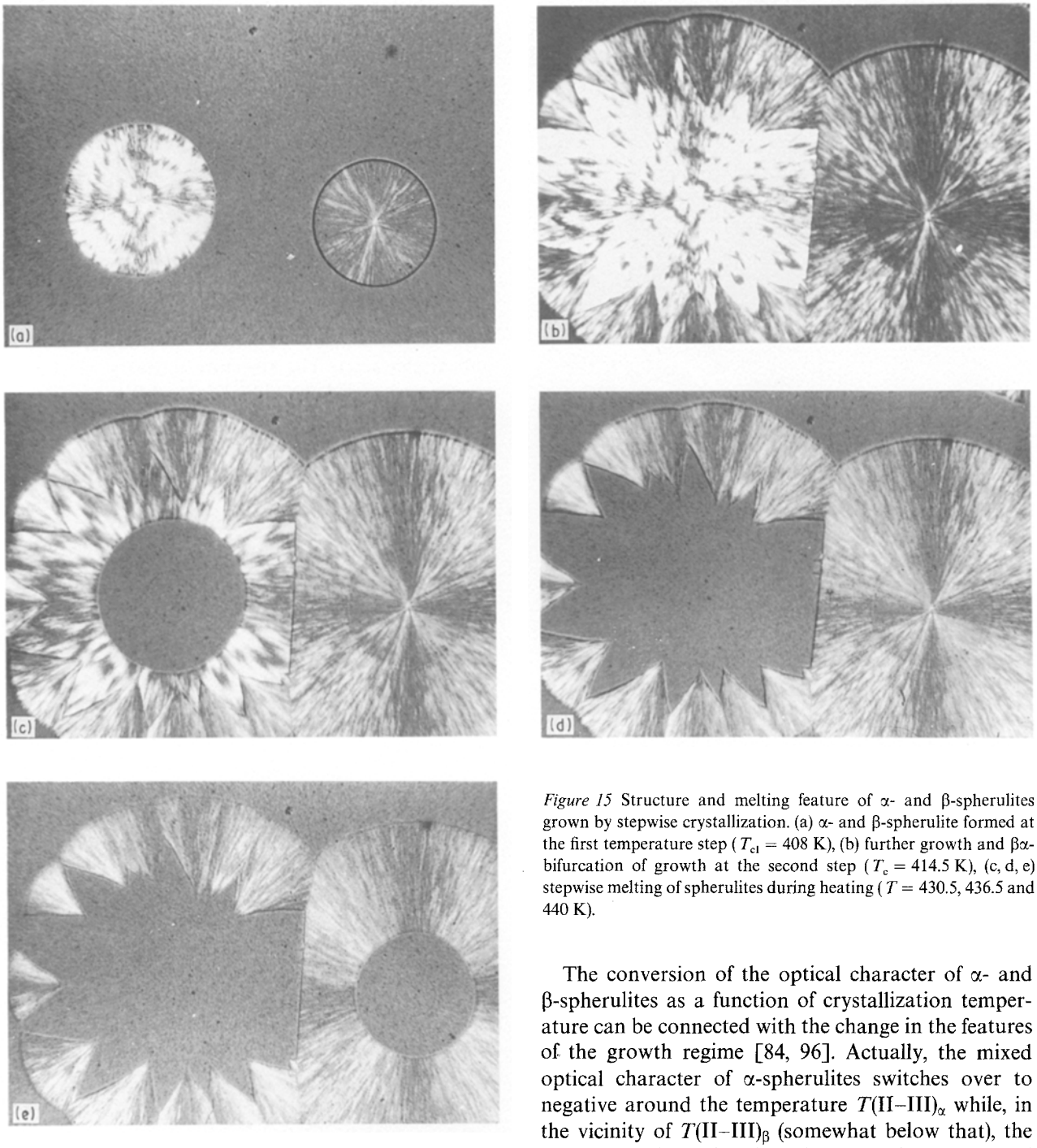

Figure 15 Structure and melting feature of α- and β-spherulites grown by stepwise crystallization. (a) α- and β-spherulite formed at the first temperature step (T_{c1} = 408 K), (b) further growth and βα-bifurcation of growth at the second step (T_c = 414.5 K), (c, d, e) stepwise melting of spherulites during heating (T = 430.5, 436.5 and 440 K).

the micrographs in Fig. 16. It is clearly visible after the complete fusion of β-modification (Fig. 16b) that the βα-bifurcation on the surface of the growing spherulite is nearly complete at this temperature. It should be emphasized that increasing temperature involves decreasing growth rates (G_α, G_β) simultaneously with increasing the number of α-nuclei.

4. The data of growth kinetics (Fig. 14) can be interpreted using the theoretical relationships of crystallization kinetics [95, 96]. It was established that growth of α and β-modifications proceed in the Hoffman's growth regimes II and III in the temperature range studied. The cross-over temperatures for the transition between the growth regimes II and III are in agreement with literature data, being $T(\text{II–III})_\alpha = 408 \pm 1$ K [84, 96] and $T(\text{II–III})_\beta = 406.2 \pm 1$ K [94] for α- and β-modifications, respectively.

The conversion of the optical character of α- and β-spherulites as a function of crystallization temperature can be connected with the change in the features of the growth regime [84, 96]. Actually, the mixed optical character of α-spherulites switches over to negative around the temperature $T(\text{II–III})_\alpha$ while, in the vicinity of $T(\text{II–III})_\beta$ (somewhat below that), the transition of β-spherulites between the radial and ringed types is observed [9, 53, 61].

5. The temperature $T_{\beta\alpha}$ = 413–414 K, above which βα-bifurcation of growth occurs during the course of step-wise crystallization, can be regarded as the theoretical upper limit temperature of formation of the β-modification, i.e. above this temperature, the formation of the β-modification is not possible. Even if a nucleus of β-modification might occur accidentally during crystallization above $T_{\beta\alpha}$ ($T_c > T_{\beta\alpha}$), no β-phase could develop due to the βα-bifurcation of growth on the surface of the nucleus.

Above the temperature $T_{\beta\alpha}$, only some further growth of the β-modification may exist, followed more and more frequently by βα-bifurcations of growth.

Lovinger *et al.* [12] observed an opposite phenomenon, αβ-bifurcation of growth, during the crystallization at a substantial undercooling ($T_c < T_{\beta\alpha}$). At a high cooling rate, a usually individual β-nucleus is

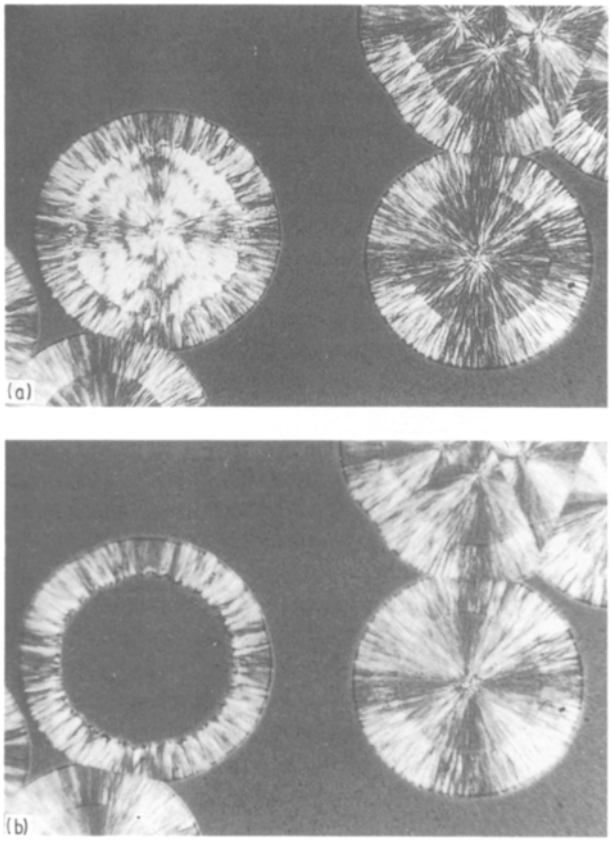

Figure 16 (a) β-spherulite grown by stepwise crystallization (T_{c1} = 408 K, T_{c2} = 418 K) and subjected to βα-bifurcation and (b) the remaining annule of α-modification after melting of the β-modification.

formed on the surface of some growing α-spherulites, which develops into a β-spherulite segment. However, this αβ-bifurcation is an accidental event, difficult to reproduce [12, 60]. It is worth mentioning that this αβ-bifurcation is utilized in the temperature gradient method by which films enriched in β-modification are prepared [10–12].

3.2. Effects of melting history

Another noteworthy thermal factor that influences the course of spherulitic crystallization and the resulting structure is the thermal history of the melt, i.e. the preceding melting conditions, final temperature, T_F, and duration, t_F, of fusion before the crystallization.

The role of fusion conditions can be attributed to the fact that, after melting of the polymeric crystallites, partially ordered molecular bundles may remain in the melt which can act as self nuclei [93] during the course of recooling. These self nuclei may induce a high-temperature crystallization called self-seeding [93].

Thermal stability of the partially ordered molecular bundles remained after the melting, depending on the characteristics of the original crystal structure. This will be illustrated by several examples later on. In this section, the effect of fusion conditions on the features of the new crystallization process is shown for initially spherulitic samples obtained by crystallization in a quiescent melt. The influence of the final temperature, T_F, of fusion on the new crystallization during the course of cooling was first studied by Vidotto *et al.* [97] for polyethylene, polyoxymethylene, and polybutene. Banks *et al.* [98] demonstrated, for partially crystallized iPP samples containing individual α-spherulites, that an aggregate of microcrystals could be resolved in place of the original spherulites molten out after the mild fusion before recooling (the structural memory effect). Binsbergen and de Lange [54] established that the elements of the aggregates were long-shaped optically positive particles oriented in the direction of the radius of the original spherulite. For this reason, the whole particulate aggregate in the place of the previous spherulite also had a positive optical character. The structure memory effect in a sample containing individual α- and β-spherulites is illustrated in a micrograph from the author's laboratory (Fig. 17). This phenomenon was studied by several research groups for samples with α-spherulites [55, 56, 73, 99].

Early reports [54, 97, 98] associated the effect of the final temperature of fusion with a partial melting of the samples, attributing it to the role of some residual crystalline phase. It is reasonable, however, to make the role of the thermal conditions somewhat more precise. As shown above, the melting of polymers proceeds in a wide temperature range and the temperature of collapse of the crystallites having the highest melting point is accepted as the experimental melting

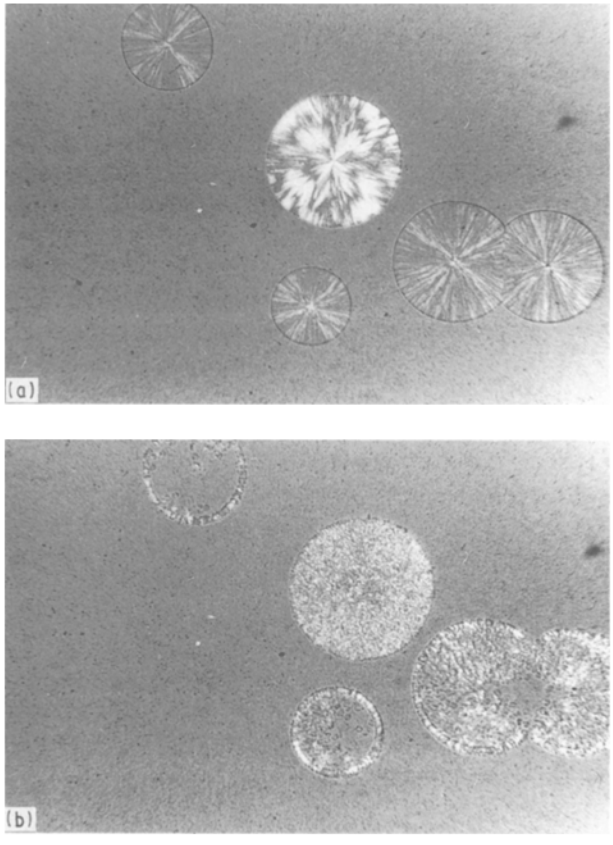

Figure 17 New crystallization of a sample containing α- and β-spherulites preceded by heating up to above the melting point of α-modification ($T_m(\alpha) < T_F$) into microcrystalline aggregates. (a) Initial sample at T_c(T_c = 408 K), (b) new crystallization during cooling after fusion.

point, T_m. If the final temperature of fusion, T_F, approximates but does not exceed T_m($T_F < T_m$), a certain proportion of the crystalline phase remains in the system which acts as crystalline self-nuclei during the subsequent cooling. If, however, $T_F > T_m$, the sample will be amorphous, i.e. no long-distance three-dimensional order will remain. This amorphous phase still cannot be regarded as an isotropic melt, because some local orderliness of the molecular chains previously included in a crystal lattice has been preserved. These clusters of local orderliness can be considered as "amorphous self-nuclei". They are able to transform into crystalline self-nuclei during the course of cooling. Beyond the melting point, a temperature limit, T_F^*, can be defined above which even the amorphous nuclei disappear and the melt transforms into an isotropic state free of all self-nuclei ("blank" melt). The level of T_F^* depends on the original structure of the sample and may be influenced by the duration of melting, t_F. If $T_F < T_F^*$, the fusion conditions affect the course of crystallization in the cooling process and thus the final structure. The latter depends on the character and amount of self-nuclei remaining because self-nuclei induce crystallization at higher temperatures than the thermal or athermal ones. These phenomena are illustrated in Fig. 18 where the calorimetric crystallization curves are shown for samples heated to different T_F levels, followed by cooling at a constant rate.

Depending on the T_F values, the following cases can be recorded [99] for the recrystallization of iPP after the fusion of α-spherulites.

1. If $T_F > T_F^*$ (blank melt), corresponding to the crystallization conditions, one of the types of spherulite shown in Fig. 10 will be formed in the cooling process, independently of T_F.

2. If $T_F < T_m$, the "crystalline nuclei" remaining in the system induce an epitaxial recrystallization of the amorphous phase obtained by partial fusion during cooling. When heated to T_F, the structure of the crystallites becomes more perfect, causing a noticeable increase in the melting point [99]. According to Padden and Keith's observations [9], in the heating process, α_I-spherulites transform into the α_{II}-form with a simultaneous decrease in birefringence. During cooling, the negative optical character persists with a continuous increase in birefringence [73, 99]. This case essentially corresponds to a high-temperature annealing (Fig. 19b).

3. If $T_m < T_F < T_F^*$, the effect of amorphous nuclei is predominant during the recrystallization. Two cases were reported [99] as observed by optical microscopy.

(i) If T_F is higher than the melting point only by 1 or 2 K, in the sites of the original spherulites, melted positive spherulites appear during cooling (Fig. 19c). Crystallization during cooling takes place like a "photographic development process": the structure corresponding to the original spherulitic one appears suddenly with a continuously enhancing birefringence as the temperature decreases. Thus, it is not the usual method of crystallization (formation and growth of nuclei) which leads to this structure.

Spherulites newly crystallized in the positive form do not change their optical character during repeated

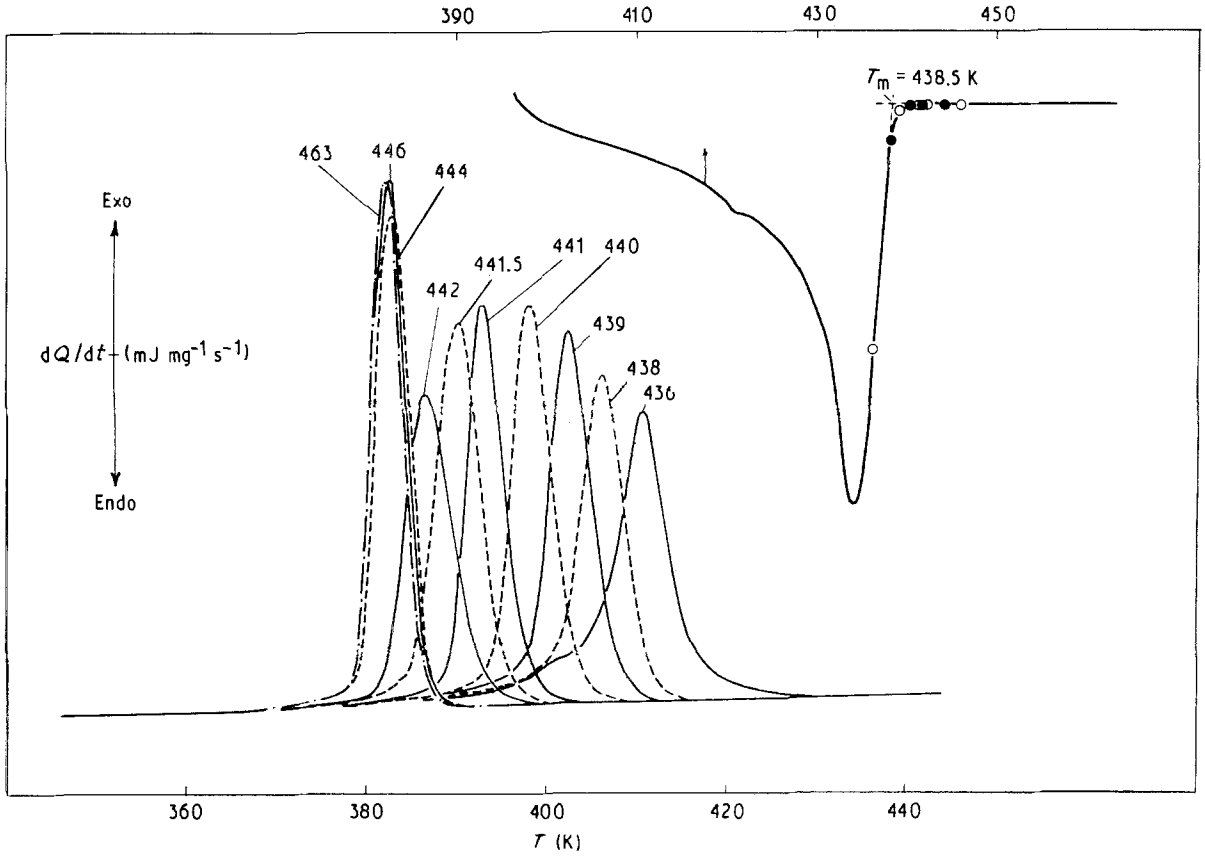

Figure 18 Effect of the final temperature of fusion on the course of recrystallization curves of a sample crystallized isothermally (T_c = 395 K for t_c = 20 min) as recorded by calorimetry. The melting curve of the initial sample is shown top right with an indication of T_F values.

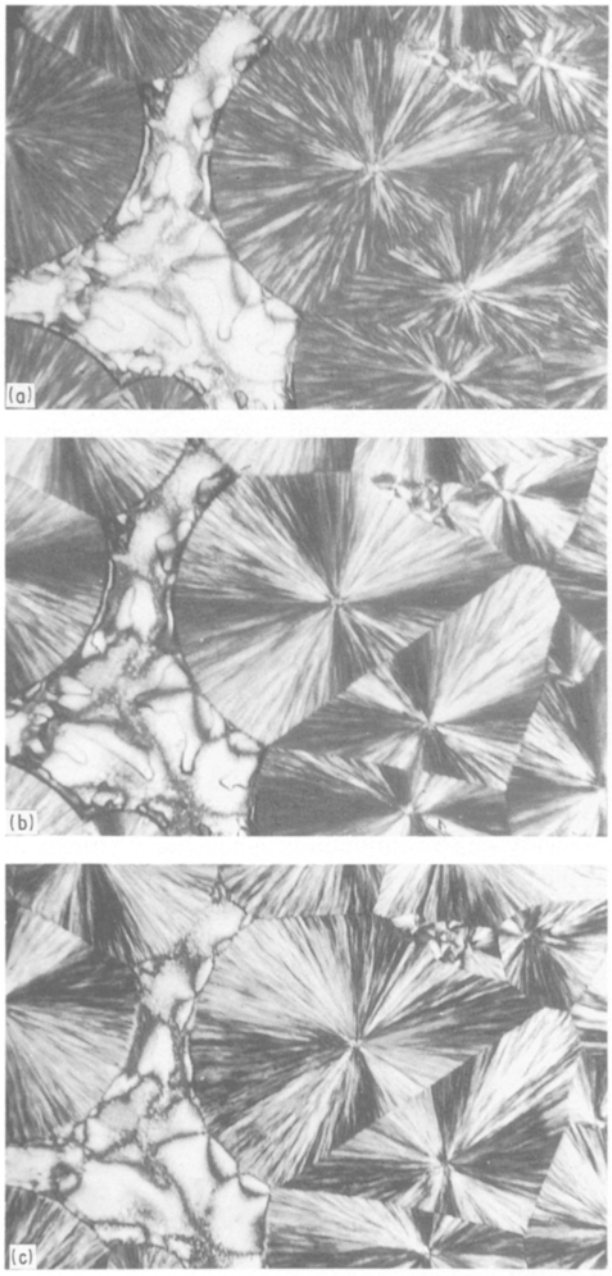

Figure 19 (a) Isothermally crystallized sample consisting of mixed α-spherulites, and its transition into (b) negative and (c) positive spherulites after heat treatment depending on T_F (see text).

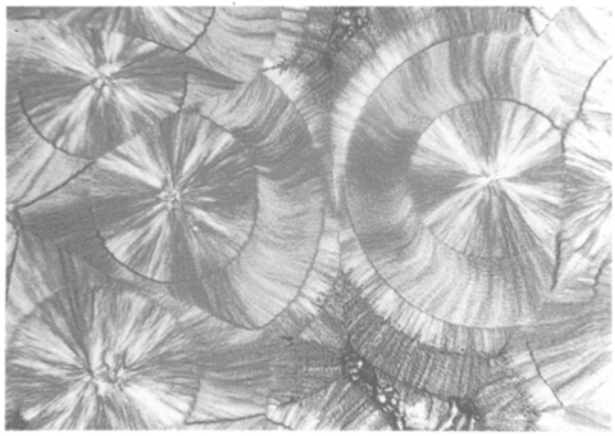

Figure 20 New crystallization of a spherulite formed on cyclically alternating the crystallization temperatures (T_c = 403, 413 K) after heating to T_F = 443 K (see text).

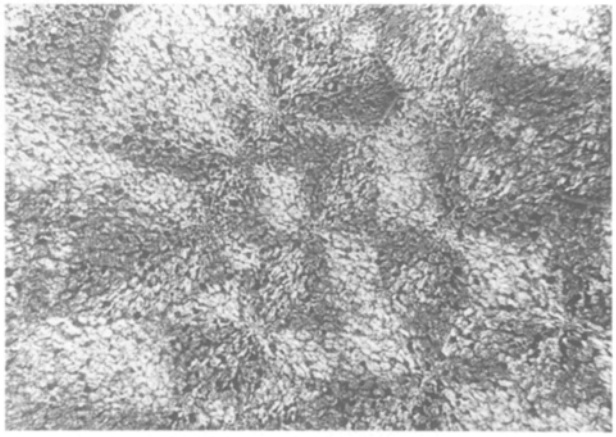

Figure 21 New crystallization of a sample consisting of α-spherulites after fusion ($T_F = T_m + 6$ K) into optically positive microcrystalline aggregates.

heating. Thus, their behaviour differs from that of the positive spherulites (α_1) formed during direct crystallization at low temperatures. Consequently, a new type of positive spherulite is formed.

As shown in Fig. 11, spherulites developed in two or more isothermal crystallization steps consist of annuli with different melting points. This type of spherulite is capable of demonstrating the above phenomena in one single sample by melting and recrystallizing them. Let T_F be selected between the melting points of the different regions. In this case, the fused part recrystallizes into an optically positive structure, while the non-melted part preserves its former negative optical character obtained during heating. It is clearly visible in Fig. 20 that the optical character of the molten regions has switched over (reversed distribution of yellow and blue fields). Recrystallization into the positive form is, therefore, a sensitive indicator for the completeness of melting.

(ii) By a gradual enhancement of T_F, optically positive microcrystalline aggregates consisting of optically resolvable individual particles replace the melted spherulites during the new crystallization by cooling (Figs 17 and 21) as shown above. As T_F is increased, the newly crystallized microcrystalline aggregates become coarser, indicating a drop in the density of self-nuclei.

In the initial stage of formation of microcrystalline aggregates, the characteristics of crystal growth from self-nuclei were studied comprehensively both by optical [54, 73, 97] and electron [54–56] microscopy. On this basis, the non-homogeneous texture of the centres of the spherulites, the origin of the positive optical character, and the cross-hatched fibrillar structure, can be interpreted during the spherulitic crystallization. It was shown [54–56] that the formation of a twin-crystalline "quadrite" structure was induced from self-nuclei. This revealed that the cross-hatched texture responsible for the positive optical character developed during the crystallization at higher supercooling [53–56]. It was also demonstrated that during an isothermal crystallization induced by self-nuclei,

optically negative and positive spherulites were formed above and below 428 K, respectively [73]. This can be attributed to the difference in the density of self-nuclei whether the new crystallization observed at the optical level takes place like a "photographic development" process or with the appearance of particular aggregates.

Recrystallization of β-spherulites after melting was studied by Varga *et al.* [100]. The new crystallization of β-spherulites is more complicated because of the melting memory effect. In the new crystallization of β-spherulites heated without recooling to different T_F, three regions with two intermediate ones can be recognized as a function of T_F.

1. If $T_F < T_m(\beta)$, β-spherulites recrystallize into the β-modification.

2. If $T_m(\beta) < T_F < T_m(\alpha)$, melted β-spherulites crystallize into optically positive spherulites of the α-modification like a photographic development process (Fig. 22).

3. If T_F exceeds the limit temperature of the self-nucleus free range ($T_F > T_F^*$), the features of recrystallization become independent of the fusion conditions.

If T_F is in the vicinity of the melting points of either β- or α-modifications, $T_m(\beta)$ or $T_m(\alpha)$, respectively, the features of crystallization and the polymorphic composition of the recrystallized sample change abruptly with T_F (intermediated regions).

Recooled β-spherulites recrystallize into the α-modification during heating and then melting in this latter form. For this reason, the features of the new crystallization as a function of T_F correspond to that described for the α-modification with a single exception; α-spherulites formed by βα-recrystallization transform into the isotropic melt state, free of self-nuclei, at a higher temperature than the original α-spherulites formed isothermally.

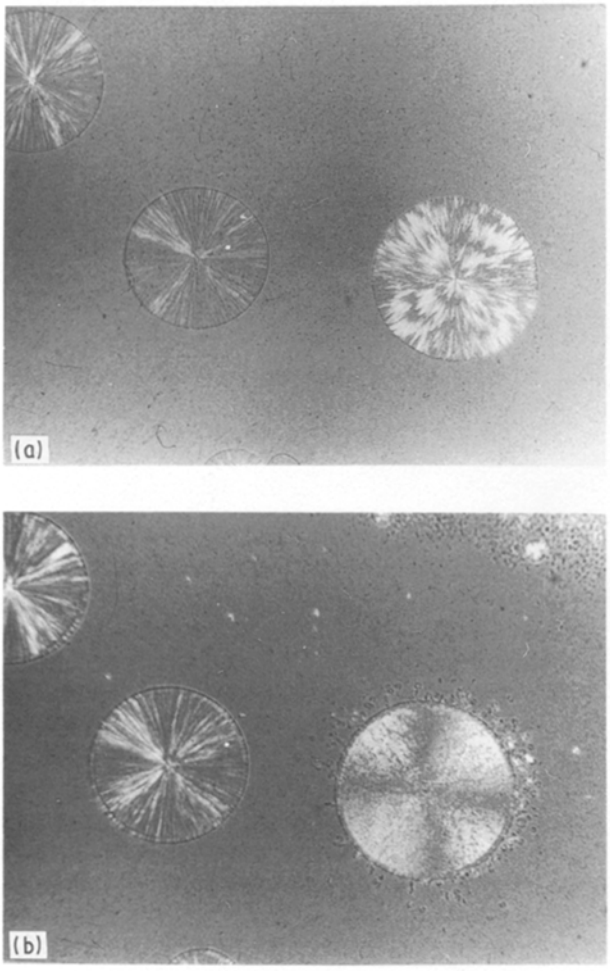

Figure 22 New crystallization of a β-spherulite (a) heated to above its melting point ($T_F = T_m(\beta) + 5$) and (b) then cooled.

3.3. Shape of spherulite boundaries

Spherulitic crystallization in a thin (essentially two-dimensional) film of a melt leads to a texture of polygonal profiles confined by straight and curved lines (Fig. 1). In a bulk crystallization, however, the spherulites are confined by planes and curved surfaces. Boundary lines and surfaces are formed when the circular or spherical spherulites, initially growing, unhindered, come into contact with each other. From this point, they can extend only in those directions where "free" melt is present.

Spherulite boundaries are "weak sites" in the polymer. Failure of the material is often initiated on these spots [101, 102]. Here cracks and voids may form during the crystallization due to some contraction (Figs 1, 3 and 11a). The "weak site" feature of spherulite boundaries is also derived from the fact that the majority of the non-crystallizing component is accumulated in these regions. Consequently, a quantitative description of the characteristics of spherulite boundaries may contribute to an exact interpretation of the fracture and failure processes.

Under isothermal conditions, the nucleation may proceed simultaneously (athermal nucleation) or at different moments (thermal nucleation). On the other hand, the linear growth rates of various polymorphic modifications are different. Because the spherulites of α- and β-modifications are formed together during the crystallization of iPP, it permits the observation of characteristics of boundary lines between spherulites nucleated at the same and/or different moments, as well as growing at different rates.

A quantitative description of boundary shapes between spherulites is given in several papers [60, 103–107]. The shape of a boundary line or surface between adjacent spherulites depends on the distance between the nuclei, on the time shift between their nucleation, and on the absolute and relative growth rates of spherulites. All the above factors are influenced by the thermal conditions of crystallization.

A quantitative description of the shape of spherulite boundaries is usually simplified to the two-dimensional isothermal crystallization, but the results can be extended to the three-dimensional growth as well. The following equations describe the boundary contours of shorter or longer range between two adjacent spherulites.

Consider a nucleus A as the origin of coordinates formed at a time $t_A = t_0$ after a nucleus B has formed at $t_B = 0$ on the axis X at a distance d from the

nucleus A. Growth rates of both spherulites are V_A and V_B, respectively ($V_A < V_B$), the relative rate is defined as $V_r = V_B/V_A < 1$.

The shape of the spherulite boundary in this general case (where $V_A \neq V_B$ and $t_A \neq 0$) is described by a fourth-degree equation [104]

$$\left(X^2 + Y^2 - \frac{2d}{1 - V_r^2} X + \frac{d^2 - V_B^2 t_0}{1 - V_r^2}\right)^2 = \left(\frac{2V_r V_B t_0}{1 - V_r^2}\right)^2 (X^2 + Y^2) \quad (3)$$

Equation 3 and some of its specific forms have reliable meanings if none of the spherulitic fronts "overgrows" other nucleus (i.e. $d > -V_A t_0$ or $d \geqslant V_B t_0$).

The graphical form of Equation 3 corresponds to two closed curves installed in each other being symmetrical to the X axis. The real spherulite boundary corresponds to the outer contour of this double curve. Consequently, the spherulite growing at a higher rate will encompass the other one, which thus becomes an inclusion. The formation of α-spherulite inclusions surrounded by β-spherulite (Fig. 23) was observed experimentally [104–107]. During the formation of an inclusion, the growing fronts of the β-spherulite meet behind the inclusion forming a straight intrinsic ββ-spherulite boundary [107]. However, inclusions are formed very rarely because other spherulites growing in the vicinity of the two nuclei prevent it occurring (Figs 24–26). The "dented" βα-spherulite boundary line in Fig. 25 has formed due to the considerable time lag of nucleation of β-spherulite with the higher growth rate.

One of the special cases ($V_A \neq V_B$ and $t_0 \neq 0$) is realized when the spherulite growing at a higher rate (A) is nucleated at the same moment that the growing front of the other spherulite reaches site A ($d = V_B t_0$). The same phenomenon is observed when a modification transition occurs in the front of the growing spherulite (βα-bifurcation of growth, cf. Fig. 15). In this case, Equation 3 simplifies to that of the limacon of Pascal [104].

If two nuclei are generated at the same moment ($t_0 = 0$) but grow at different rates, being different in modification ($V_A \neq V_B$), the boundary line between them will be circular, as described by the following equation

$$\left[X - \frac{d}{(1 - V_r^2)}\right]^2 + Y^2 = \left[\frac{dV_r}{(1 - V_r^2)}\right]^2 \quad (4)$$

This circular spherulite boundary (formation of an incomplete inclusion) is illustrated in Fig. 26. It can be

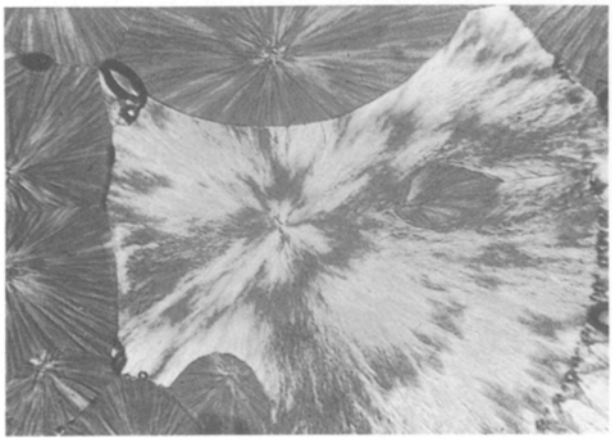

Figure 23 A ringed spherulite enclosing an inclusion of leaf-shaped β-spherulite (T_c = 397 K).

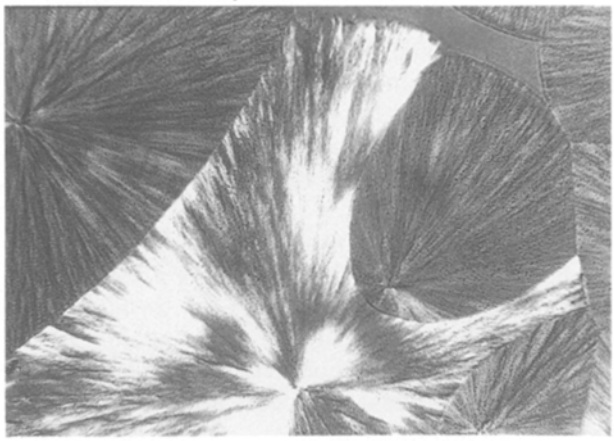

Figure 24 Partial formation of an α-inclusion in a mixed polymorphic sample (T_c = 397 K).

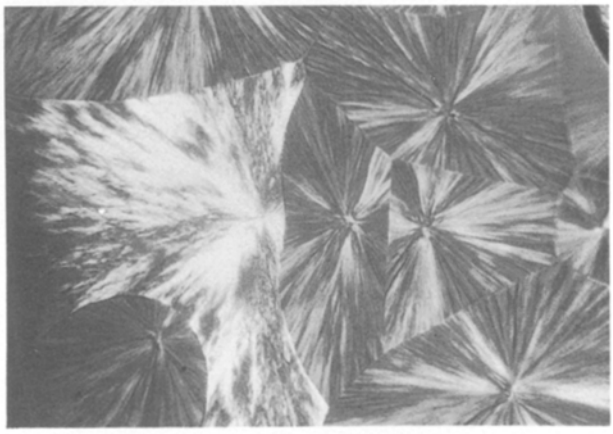

Figure 25 Pattern of a "dented" boundary line between α- and β-spherulites (T_c = 395 K).

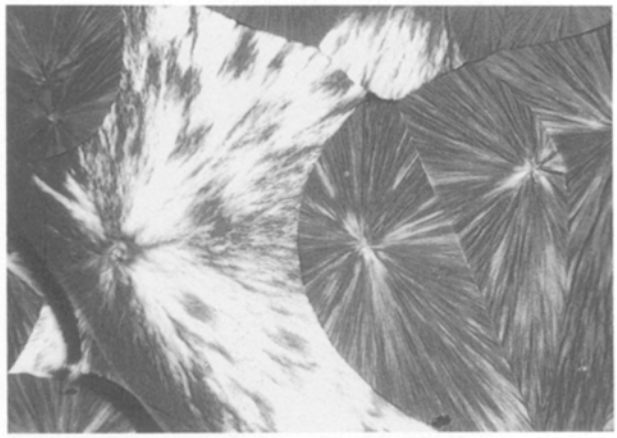

Figure 26 Pattern of a circular boundary line between α- and β-spherulites (T_c = 395 K).

seen that the original nucleus is not situated in the centre of the round-shaped spherulite inclusion, while the optical centre of the inclusion is coincident with the original nucleus.

Spherulites growing at the same rate (identical modification) form hyperbolic ($V_A = V_B$ and $t_0 \neq 0$) or straightline ($V_A = V_B$ and $t_0 = 0$) boundaries. The simplified forms of Equation 3 for these cases are

$$\left(X - \frac{d}{2}\right)^2 \Big/ \left(\frac{Vt_0}{2}\right)^2 - \frac{Y^2}{\left[\left(\frac{d}{2}\right)^2 - \left(\frac{Vt_0}{2}\right)^2\right]} = 1 \quad (5)$$

$$X = \frac{d}{2} \quad (6)$$

Experimentally, the wing of the hyperbola of Equation 5 that has the nucleus formed later in its focus will appear. The straight-line boundary corresponds to the normal bisector of the junction line between the nuclei. These two latter cases are the most frequent phenomena in the spherulitic crystallization, as illustrated in Fig. 27.

The experimentally observed shape of inclusions differs from that expected from the above deductions [104, 105]. They are leaf-shaped ending in a tip (Fig. 23). This is attributed to the fact that the front of the spherulite travels a longer way than expected from the deduction of Equation 3 when an inclusion has been formed [104]. By drawing a tangent from the nucleus of the faster-growing spherulite to the actual spherulite boundary, a shielding point is marked out. At this point, the spherulite front growing from the nucleus A is shaded by the spherulite formed from the nucleus B causing a distortion of the shape of the front. The role of this shielding point was first demonstrated by Ledniczky [105] who later attempted to develop an approximate quantitative description [106]. The exact solution of this problem was attained by Schulze and Wilbert [107] revealing that the distorted spherulite front behind the shielding point follows a logarithmic spiral in shape. The shape of the spherulite boundary behind the shielding point is also described by two logarithmic spiral curves symmetrically to the straight line between nuclei A and B. The boundary between the spherulites from nuclei on the growing spherulite fronts and the basic spherulite, also forms two logarithmic spiral sections in contrast to the limacon of Pascal [60, 104] given by disregarding the shielding effect. Thus, Equations 3 and 4 are valid up to the shielding point. Because several nuclei may be situated in the vicinity of a given spherulite, the boundary sections between the individual pairs of nuclei do not extend to the shielding point in the majority of cases. Consequently, the applicability of Equations 3 and 4 is practically not limited by the aforementioned limit of validity, apart from the very rare formation of inclusions.

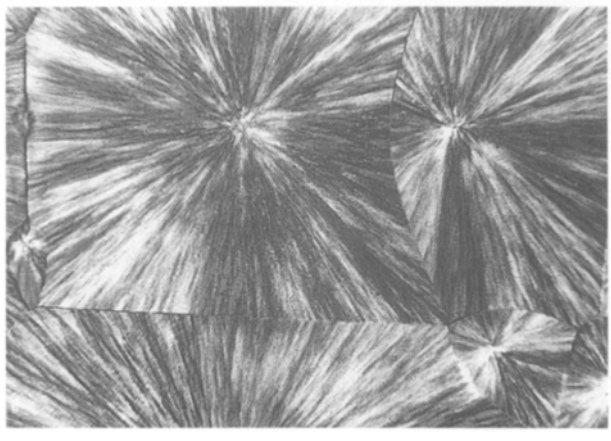

Figure 27 Linear and hyperbolic boundary lines between α-spherulites.

4. Cylindritic crystallization of iPP

Mechanical stresses (tension, shear, compression) exert considerable influence on the crystallization of molten polymers and on the features of the supermolecular structure formed. The mechanical effects act essentially on the elementary processes of nucleation. By tensile and shear loads, polymeric molecules are stretched and oriented into rows in the molten state. These prearranged rows of molecules transform into crystalline clusters at a certain temperature which may act as crystallization nuclei. This characteristic linear type of self-nucleus is termed a row nucleus [108, 109]. Row nuclei begin to crystallize at a higher temperature than the homogeneous or heterogeneous ones. Row nuclei induce an epitaxial growth of crystallites of folded chains leading to characteristic supermolecular formations of cylindrical symmetry, cylindrites [109]. Thus, the core of a cylindrite is a row nucleus which develops into folded-chain fibrillar crystallites perpendicular to the row at cylindrical symmetry [108]. Like the spherulites, these growing folded-chain fibrillar crytallites may also branch, providing complete space filling. The fibrils can be either linear or helical (twisted around their longitudinal axis) as in the case of the radial or ringed spherulites, respectively. The diameter of the row nuclei in the cylindrites is estimated to about 15 nm, while the size of fibrils may reach the micrometre range [110] like that of the building units in the spherulites. The dimension ratios of the cylindritic structural elements are markedly different from the "shish-kebab"-type formations where the diameter of the stretched-chain fibrils and the dimensions of the folded-chain lamellae on them are commensurable.

During the crystallization of iPP, well-developed cylindritic structure, resolved by optical microscopy, may be formed. Even a slight shear stress of molten iPP leads to a cylindritic crystallization [111–113] as demonstrated by the series of pictures in Fig. 28. In a molten thin film between glass plates, row nuclei are formed when a shear stress is applied by slipping the cover plate. For the sake of testing technique, it is reasonable to distinguish three types of row nucleus density: row nucleus density is high if the diameter of the cylindrites on the row nuclei remains below the optical resolution; at medium row nucleus density, cylindrites are readily distinguishable at the optical level (Fig. 28); a sample has low row nucleus density

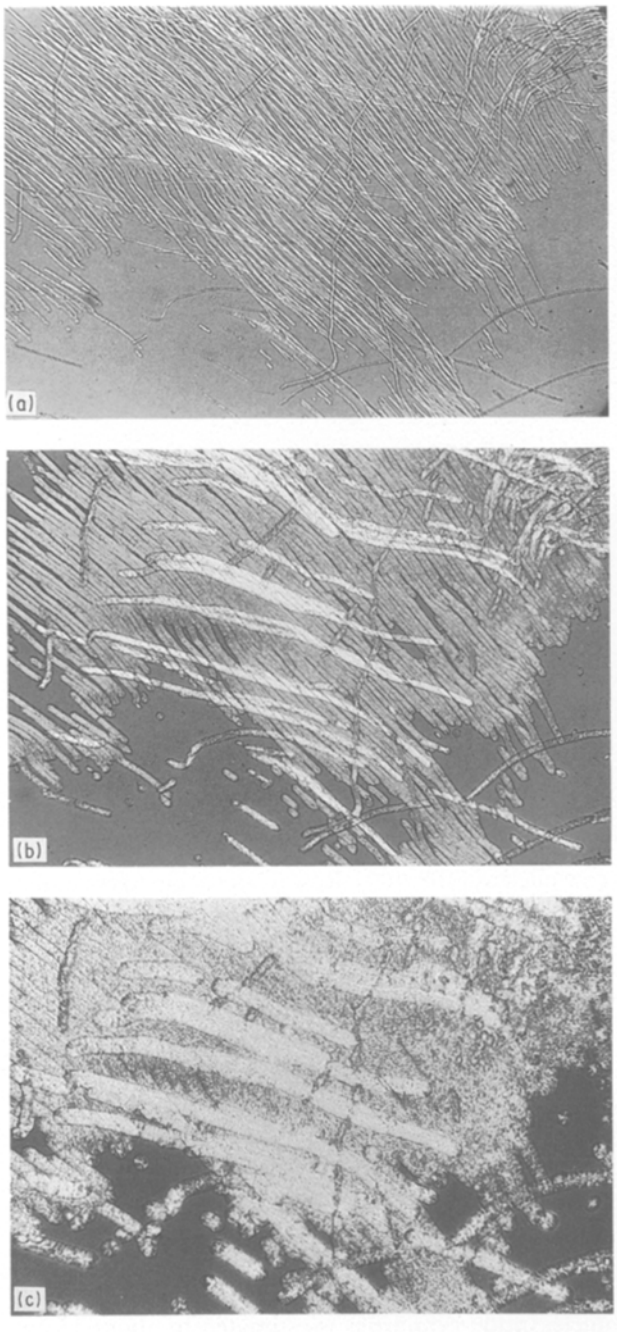

Figure 28 Cylindritic crystallization (a–c) in slightly sheared melt ($T_c = 403$ K).

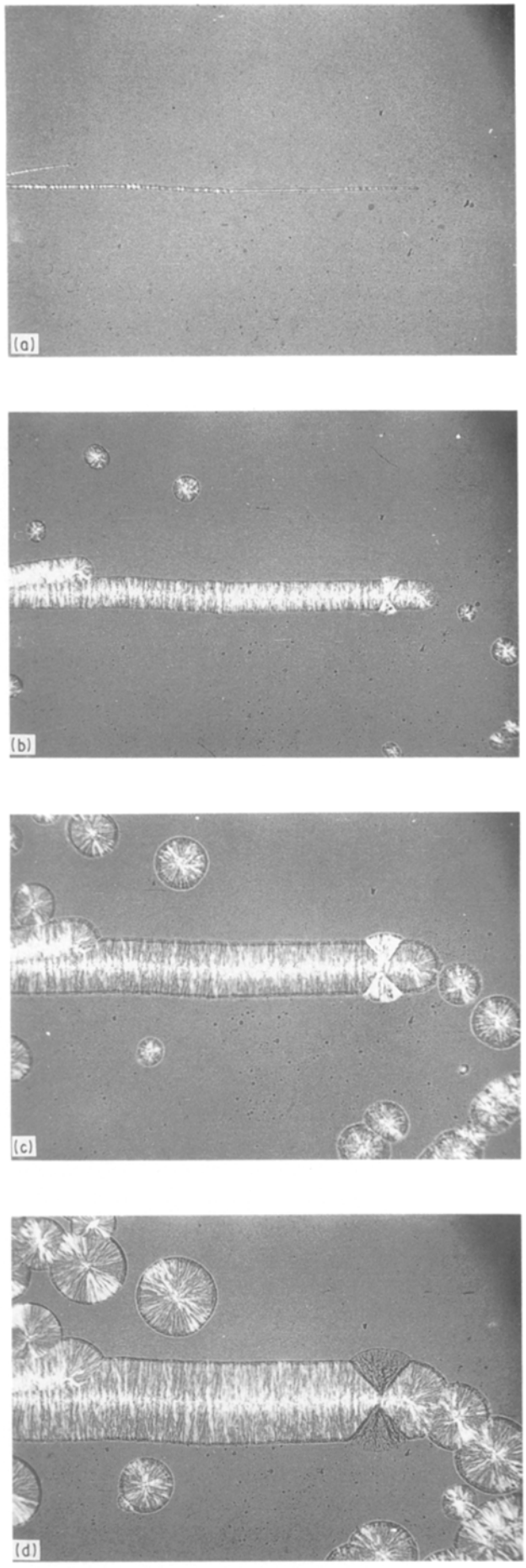

Figure 29 Cylindritic crystallization on stable row nuclei ($T_c = 403$ K), (a) after cooling to T_c, (b, c) isothermal growth at 403 K, (d) after the segment of β-spherulites has molten out when heated to 430 K.

when only a few isolated individual cylindrites appear (Fig. 29). Characteristics of cylindritic crystallization can be visualized most clearly in samples of the latter type.

Characteristic features of the cylindritic crystallization are summarized as follows [113].

Row nuclei have considerable thermal stability in a relatively wide temperature range above the melting point. Consequently, a marked structural memory effect can be observed in the cylindritic crystallization. In other words, after repeated consecutive melting–cooling (fusion–recrystallization) cycles, the cylindritic structure is reproducibly recovered. The thermal stability of row nuclei and the reproducibility of cylindritic structures were studied by Varga [113]. He established the following cases depending on the final temperature of fusion, T_F:

(i) $T_m < T_F < (T_m + 15\ K)$ – row nuclei are thermally stable and the fused sample crystallizes into the original cylindritic structure when cooled;

(ii) $(T_m + 15\ K) < T_F < 473\ K$ – the number of row nuclei gradually decreases and nuclei are observed to break into pieces. The stability of row nuclei is determined in this range by the mechanical effects that have induced their formation;

(iii) $T_F > 473\ K$ – row nuclei are completely disintegrated and a blank melt, free of any self nuclei, is obtained. During the crystallization after fusion, therefore, a spherulitic structure is formed at an overall reduction in nucleus density. Thus, the temperature of complete disintegration of row nuclei formed in the sheared polymer melt, T_F^*, is quite high.

The course of cylindritic crystallization is illustrated by the series of pictures in Fig. 29. In the central line of the photograph, a row nucleus of high thermal stability is situated which induces cylindritic crystallization upon cooling. The cylindritic front grows in two directions, parallel to the row nucleus, resembling to a transcrystallization. At a low row nucleus density, spherulites also appear in the sample (generally at a considerable delay) resulting in a mixed cylindritic–spherulitic structure. Row nuclei induce cylindrites of α-modification. This can be explained by the fact that crystallization starts on the row nuclei at a high temperature, above the upper limit temperature of β-modification, $T_{\beta\alpha}$, thus, the formation of α-modification is inevitable. Therefore, no way leads to the formation of cylindrites of β-modification. At a high undercooling, however, punctiform β-nuclei may also be formed on a row nucleus of α-modification or on the growing α-cylindritic front. They may develop into β-spherulitic segments contoured by straight lines. From a β-nucleus on the row nucleus, the spherulitic segment grows in both directions (Fig. 29). A β-nucleus on the growing cylindritic front (αβ-bifurcation of growth) is able to grow only in one direction [113]. With increased undercooling, the number of β-nuclei is enhanced. At low temperatures, the great number of β-spherulitic segments may completely prevent growth of the α-cylindritic front (see, for example, Fig. 33 later). In this case, the pattern of the sample resembles a β-cylindrite, but the stack of β-spherulitic segments grown from individual nuclei is proved by melting tests.

Because the building units of both cylindrites and spherulites are folded-chain fibrils [108], differing only in steric arrangement from one another, many common features can be observed in the crystallization, melting, and optical characteristics of cylindrites and spherulites and in their dependence on the thermal conditions. The only exception is a narrow region of the cylindrite in the close vicinity of the row nucleus due to the fact that crystallization starts earlier (at a higher temperature, before reaching the isothermal T_c) on the row nuclei. It was demonstrated experimentally [113] that growth rates of spherulitic and cylindritic fronts of identical modification were equal. The dependence of the optical character of α-cylindrites on T_c is the same as that of spherulites: negative above 410 K, while, below this temperature, cylindrites of mixed optical character are formed. Positive cylindrites were found in highly undercoolable random copolymers of ethylene and propylene.

At the same time, the cylindrite region in the close vicinity of an α-row nucleus is always negative optically. Between crossed polarizers at a diagonal position parallel to the γ axis of the λ plate, negative cylindrites are blue, positive ones are yellow while, in mixed cylindrites, blue and yellow stripes alternate irregularly perpendicular to the row nucleus (Fig. 30). α-cylindrites, produced by stepwise crystallization, consist of stripes of optical character corresponding to T_c, and melt stepwise. Changes in the optical character of cylindrites during the recrystallization after annealing or melting as a function of T_F are identical to

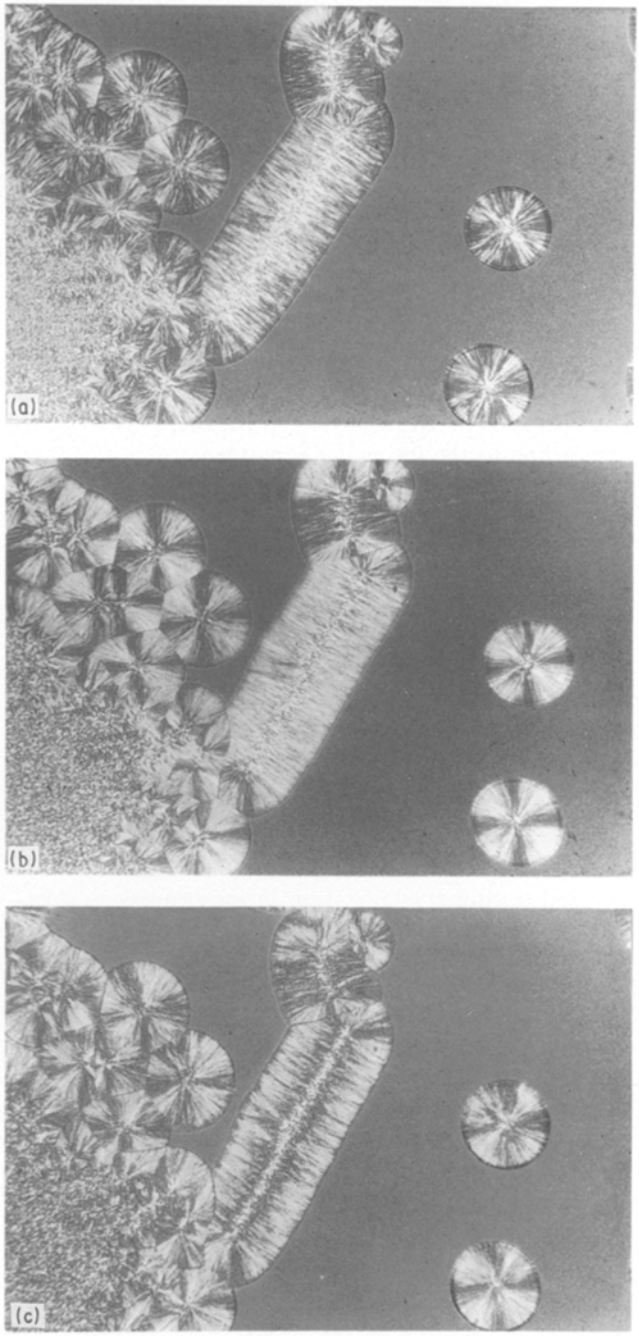

Figure 30 (a) Cylindrite of mixed optical character crystallized isothermally ($T_c = 403$ K), and its transition into (b) negative ($T_F < T_m$) or (c) positive ($T_F = T_m + 2$ K) form by heating and subsequent cooling.

those of spherulites [99] as shown by the photographs in Fig. 30. If $T_F < T_m$, the mixed cylindrites transform to negative optical character (Fig. 30a and b). When, however, the sample which was heated above T_m by 1 or 2 K and cooled down is crystallized, an optically positive cylindrite will be formed (Fig. 30a and c). It should be noted that, in the latter case, the region of the cylindrite in the close vicinity to the row nucleus would not melt; consequently, its negative optical character is preserved (Fig. 30).

In a sample containing cylindrite and spherulites together, boundary lines of characteristic shape are formed between the two types of supermolecular formation [113]. Between cylindrites and spherulites of identical modification and growth rate, the boundary line is parabolic. The shape of this parabola is determined by the relative position of the spherulitic nucleus and is independent of the growth rate and of the crystallization temperature. If the growth rate of cylindrites is different from that of spherulites, $V_c < V_s$ or $V_c > V_s$, the shape of the boundary line is a hyperbola or ellypsis, respectively. Because in iPP only α-cylindrites are formed, the boundary lines are parabolic with α-spherulites and hyperbolic with β-spherulites [113]. As was shown above (Fig. 29), straight-line boundaries may also be formed if a faster-growing spherulitic nucleus (β-modification of iPP below $T_{\beta\alpha}$) is initiated on the row nucleus or on the growing cylindritic front. The angle, φ, between the direction of the row nucleus and the straight boundary line depends on the relative growth rate ($V_r = V_c/V_s$) according to the following equation

$$V_r = \pm \frac{1}{\cos\varphi} \tag{7}$$

It is worth mentioning that boundary lines between transcrystallization fronts developing from heterogeneous surfaces and spherulites, are similar to those described above.

5. Structures crystallized under processing conditions

The structure of crystalline polymeric products is formed during crystallization in the processing operations and depends on the thermal and mechanical conditions in the mould cavity. These conditions are highly influenced by the parameters of the processing technology. In addition, thermal and mechanical conditions vary locally according to the geometry of the mould cavity. Consequently, products (except for compression-moulded ones) have non-homogeneous anisotropic structure [114] with properties varying within a wide range depending on the processing factors.

Many reports covered determination of structures and properties of products as functions of the processing conditions. The present paper treats only the supermolecular level of the structure as studied by optical microscopy. It should be emphasized that optical microscopy provides useful information about the structure of a sample as a whole, in spite of its relatively low resolution. Possibilities of optical studies can be widened by extending them to the observation of melting and recrystallization processes, i.e. thermo-optical methods are used. In our laboratory, a thermo-optical technique was developed based on the structural memory effect [115] for testing end-products. As shown above, the structural memory effect can be ascribed to a certain thermal stability of nuclei and remnants of various supermolecular structures above the melting point acting as self-nuclei during recooling of the melt. Self-nuclei of different types may have considerably different thermal stabilities. Residues of folded-chain crystallites setting up spherulites and cylindrites are stable only in a very narrow temperature range ($\Delta T_F = T_F^* - T_m \cong 6.0$ K) [99] while row nuclei (or their fragments) formed by mechanical effects remain in a molten polymer more or less even up to $T_F = 473$ K [113]. Stability of row nuclei is also influenced by the intensity of the mechanical effect that has induced their formation, governing the dimensions and order of rows of molecules formed. Thus, a systematic variation in the final temperature of fusion, T_F, may "develop" morphological formations of different stability separately by means of the new crystallization. A direct observation of crystallization under the processing conditions involves technical difficulties. For this reason, only indirect information is available about the process of structure formation. The thermo-optical method based on the structural memory effect provides an essential reconstruction of the crystallization process during the moulding [115].

5.1. Structure of injection-moulded products

Injection moulding involves particularly complicated thermal and orientation conditions during cavity filling. These deformation and orientation processes are generally accepted to be described by the Tadmor model [116]. Accordingly, surface layers of flowing melt are exposed to tensile stress while lower layers suffer shear stress, resulting in an orientation of molecular coils in the flow direction. In the core, further from the wall, some extent of disorientation may take place after cavity filling and before crystallization, depending on the heat-transfer conditions. All these processes lead to a complex non-homogeneous supermolecular structure from the crystallizing polymers. Kantz *et al.* [117] were the first to demonstrate that injection-moulded iPP had a skin–core structure. This skin–core structure and the relations between structure and properties were studied by several groups [115, 117–135]. They suggested various models to describe this complex structure on the basis of optical microscopy, X-ray diffraction, electron microscopy, and calorimetry. The supermolecular structure of a microtomed section from an injection-moulded sample cut at the machine direction is illustrated by an optical micrograph in Fig. 31. It can be seen that the core layer has a spherulitic structure demonstrating a disorientation (relaxation) of the melt in this region before crystallization has started, followed by a crystallization in the quiescent melt. The

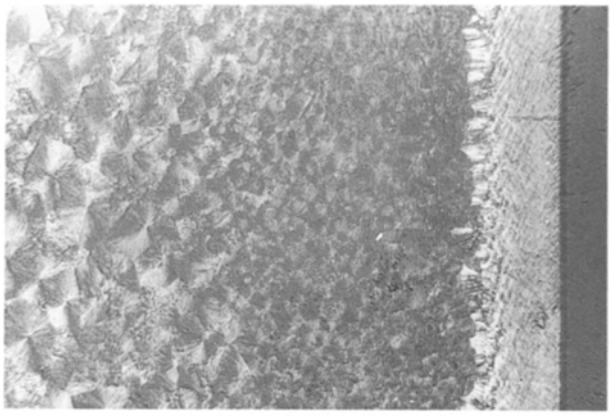

Figure 31 Characteristic skin–core structure of injection-moulded iPP.

largest spherulites are found at the centre of the sample, and the size decreases towards the wall of the mould reflecting the heat-transfer (cooling) conditions in the cavity. The skin layer is highly oriented having a homogeneous structure at the resolution level of optical microscopy and a negative optical character with unrecognizable individual morphological formations. Between the core and skin layers, a relatively sharp boundary line appears (Fig. 31).

It was revealed by thermo-optical investigations based on the structural memory effect that the sheared region consisted of α-cylindrites of negative optical character oriented in the machine direction with diameters less than the resolution level of optical microscopy, due to the high density of row nuclei. In a sample newly crystallized after heating above the melting point (T_F = 448 K), cylindritic structure is resolved even at the optical level (Fig. 32). It seems probable from the observation of recrystallization that a rapid cylindric crystallization proceeds on row nuclei formed in the sheared region during the processing. From this layer, a transcrystalline front grows towards the core of the sample where spherulitic crystallization starts after a significant delay. Consequently, the relatively sharp boundary layer between the skin and core layers is an outcome of the transcrystalline front. As is clear from the micrographs in Fig. 32, the majority of the transcrystalline part of the sample is of α-modification with sporadic β-spherulitic segments confined by straight lines. Formation of these segments is induced by β-nuclei appearing on the surface of the transcrystalline front as evidenced by the straight-line βα-boundary line [113]. By increasing the cooling rate, the β proportion of the transcrystalline phase is enhanced. As indicated by the sections from the end-product (Fig. 31), the greater part of the transcrystalline region is formed in β-modification under injection moulding conditions [115, 135]. The structure of the skin layer is, therefore, complex comprising the extended outer layer, the cylindritic region oriented in the machine direction in the sheared zone, and the transcrystallized zone growing down the latter. Depending on the technological parameters of injection moulding, the thickness of the complex skin usually varies between 100 and 350 μm.

The existence of a tensile stress on the surface of the flowing melt is indicated by a characteristic structure along the weld lines [115]. It is clearly perceptible in Fig. 33 that highly birefringent β-segments have grown down from the parabolic weld line. It can be established on the basis of the optical pattern and of the melting characteristics that the immediate surroundings of weld lines are of α-modification consisting of row nuclei originated by extending the surface layers and of a cylindritic structure formed thereon. By virtue of the row nuclei on the surface, the earliest crystallization takes place on this site. Even in this case, β-spherulitic segments are induced by β-nuclei formed on row nuclei that lock the growth of the α-cylindritic front due to their higher growth rate. According to the melting and recrystallization experiments, the thermal stability of row nuclei formed by virtue of the extension in the surface layers, is markedly lower than that in the sheared region, indicating the differences in the mechanical stress. It is worth pointing out that the angle, φ, between the βα-boundary line formed during the transcrystallization and the row nuclei, depends on the relative growth rate ($V_r = V_\alpha / V_\beta$) (Equation 7) which is, in turn, temperature dependent. With a knowledge of the temperature function of V_r, the crystallization temperature can be determined from angle φ. In other words, angle φ may serve as an "internal thermometer".

Ehrenstein *et al.* [136] developed a method of manufacturing high-strength greatly oriented (self-reinforced) plastic products using conventional processing machines (such as injection-moulding machines). Thermo-optical investigations revealed a high density of negative cylindrites oriented in the machine direction in self-reinforced iPP injection mouldings, without a spherulitic core in contrast to the skin–core structures of conventional injection-moulded products.

5.2. Structure of extruded products

According to the investigations of Dragaun and Muschik [137–139], extruded products have also skin–core structure. Similarly to injection mouldings, the skin structure is homogeneous at the optical level while the core consists purely of α-spherulites. The thickness of the skin layer depends on the temperature difference (ΔT) between the melt and the cooling bath but never exceeds 300 μm. Skin thickness decreases slightly with increasing ΔT. The area surrounding the sheared region is rich in partially oriented spherulites of β_{III} type, as in injection-moulded samples. The skin layer has also formed by oriented crystallization on row nuclei due to the shear stress in this case. Thermo-optical studies [140] based on the structural memory effect revealed that the skin layer of iPP extrudates consisted of optically negative cylindrites again oriented in the machine direction. It was proved by the fact that the recrystallization of a sample fused under mild conditions ($T_F = T_m + 15$ K) before recooling proceeded in a similar way to that of the injection mouldings (Fig. 32).

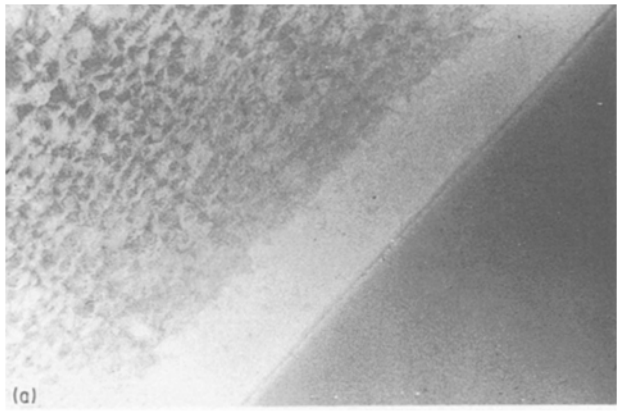

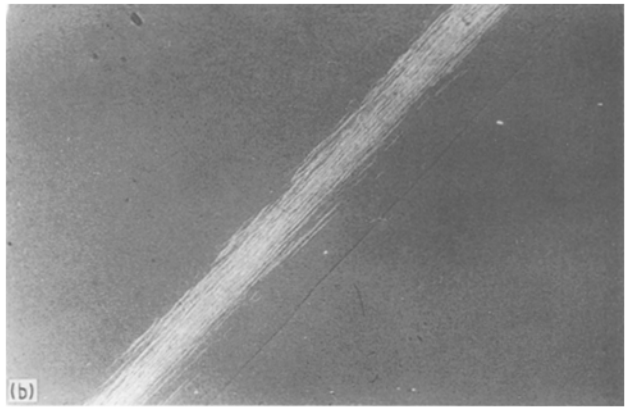

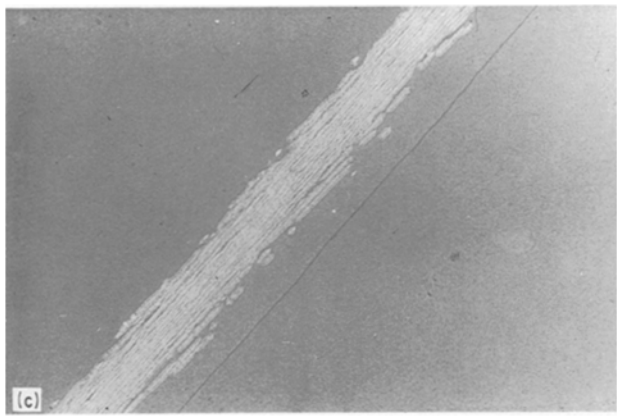

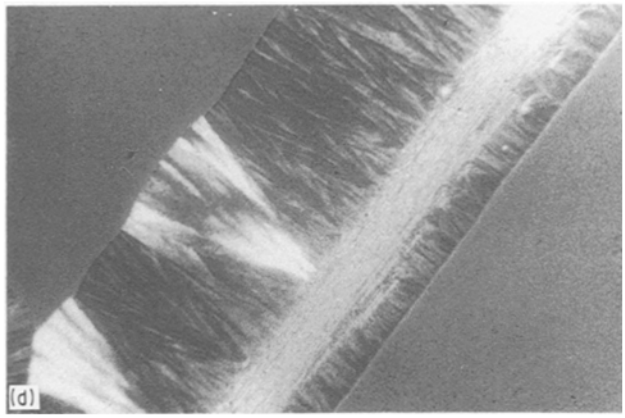

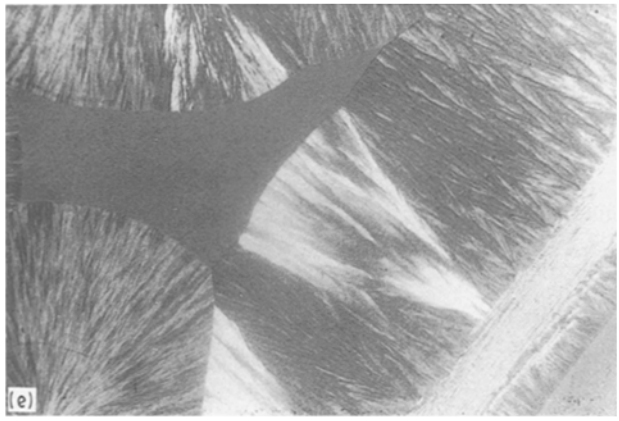

Figure 32 Section from injection-moulded sheet and its new crystallization after heating (T_F = 448 K). (a) Initial sample; (b, c, d) during the cooling process at 418, 416, 410 K after fusion at 448 K; (e) isothermal crystallization at 410 K.

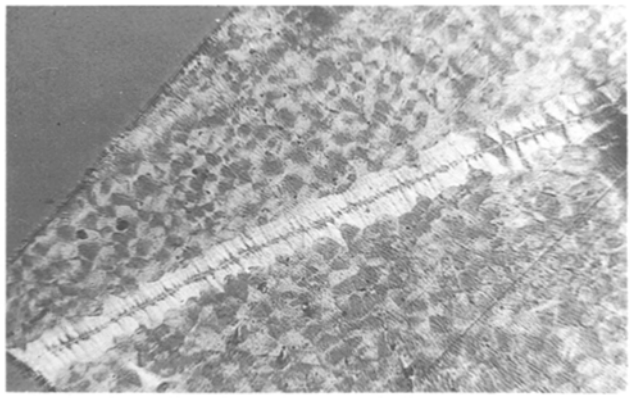

Figure 33 Cylindritic structure containing a large number of β-spherulitic segments formed along the weld line.

5.3. Structure of weld joints

Large-scale mass production of plastic bulk goods renders high significance to the various welding techniques. PP products are usually joined by hot-plate welding or vibration welding. In the processes, surface layers of parts to be joined are melted followed by cooling under a predetermined pressure. Bond strength is provided by the crystalline structure formed in cooling the melt. Welding conditions (temperature, pressure, duration) control the temperature distribution and flow conditions from site to site. On the other hand, the thermal environment and mechanical stress considerably affect the structure formed after recrystallization and, consequently, the bond strength.

The theoretical basis of hot-plate welding was analysed comprehensively by Potente [141]. The supermolecular structure of weld joints in iPP and its dependence on the welding parameters have been covered by several papers [142–150]. The supermolecular structure of joints is complex and inhomogeneous. It should be noted that, in spite of the close similarity in joint structures reported by various authors, nomenclature and interpretation of these morphological structures is far from uniform at present. The majority of joints of hot-plate welding has spherulitic structure [147], i.e. recrystallization takes place essentially in a quiescent melt. Along the central line of a joint (in the area surrounding bonded surfaces), a band of spherulites [143] (or a "dendrite" structure as

stated by Korub [142]) can be observed in most cases. In our opinion, this can be deduced from a higher density of heterogeneous nuclei due to the contamination (possibly partial decomposition) of the surface to be bonded. Symmetrically to the central line, two spherulitic regions can be seen [147] mostly with the α-modification disseminated by some accidental β-spherulites (β_{III}). From the central line towards the intact material, the size of the spherulites decreases, transforming them to a microspherulitic structure. The size of spherulites and the proportion of β-modification depend on the welding conditions in this region. Between the original material and the recrystallized joint, a characteristic structure can be recognized. In the close vicinity of the intact material, an optically unresolved homogeneous zone exists highly oriented towards the edges. In our opinion, this zone consists of spherulites that melted partially and deformed by virtue of pressure (as they are plated and shifted slightly towards the edges of the sample). This assumption has been made probable by studies of the influence of the final temperature of fusion on the recrystallized structure [99].

The structure of vibration-weld joints was investigated extensively by Ehrenstein *et al.* [151–153] as a function of welding time and pressure. This method permits a considerably wider pressure range for the examination of joint formation. Thermal and rheological conditions in a weld joint and their dependence on the processing conditions were analysed by Potente [154]. It was established by Schlarb [153], extending his studies on the structure of joints by thermo-optical investigations on the basis of the structural memory effect, that three characteristic types of joint can be recognized depending on the pressure. At high pressures, the highly oriented structure formed consists mainly of cylindrites oriented to the flow direction (Fig. 34). At medium pressures, the unoriented homogeneous structure formed cannot be resolved at optical level. At low pressures, a multilayer weld structure is formed consisting of different characteristic zones (Fig. 35). Transcrystalline zones of α- or α- and β-modifications may play an important role in the formation of this structure [152]. It was also assumed that the formation of a multilayer weld structure might be associated with the facts that the layer in close vicinity to the intact material in the molten region was plastic at low pressures while those around the central line were subjected to flow deformation [152]. The optimum strength of structural joints can be attained in the range of low welding pressures.

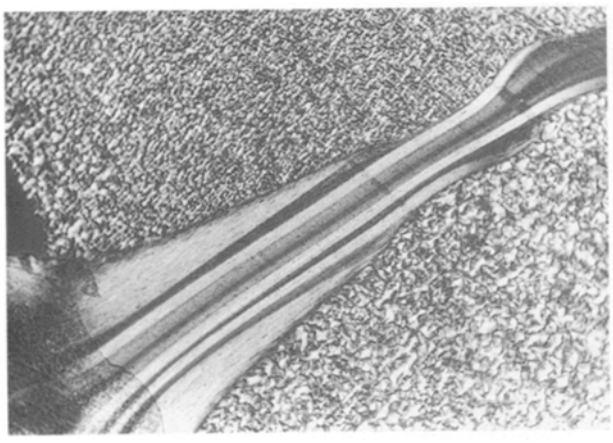

Figure 34 Highly oriented weld structure formed at high pressure.

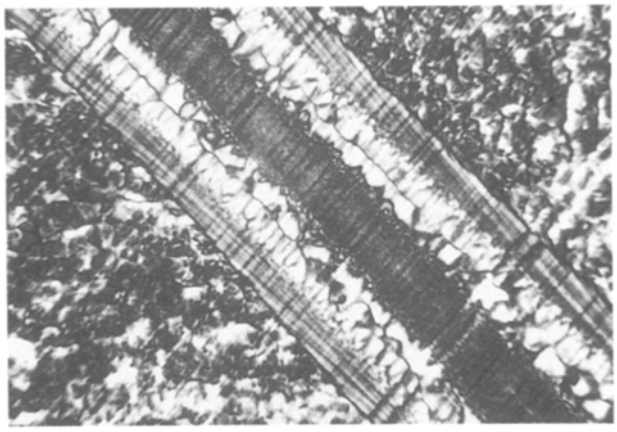

Figure 35 Multilayer weld structure (consisting of deformed spherulitic, transcrystalline and flow zones) formed at low pressure.

6. Conclusion

The supermolecular structure of isotactic polypropylene is extremely variegated as formed under different thermal conditions and mechanical stress during the crystallization process. A survey is given of the effects of the thermal conditions (crystallization temperatures, cooling rate, annealing, final temperature of fusion) on structural features of spherulites. Characteristics of the cylindritic structure formed in melts under mechanical stress are introduced. The complex character of a supermolecular structure formed under processing conditions is also analysed briefly.

References

1. P. H. GEIL, "Polymer Single Crystals" (Interscience, New York, London, Sydney, 1963).
2. D. FOX, M. M. LABES and A. WEISSBERGER, "Physics and Chemistry of the Organic Solid State" (Interscience, New York, London, 1965) Ch. 8.
3. B. WUNDERLICH, "Macromolecular Physics", Vol. 1 (Academic Press, New York, San Francisco, London, 1976).
4. R. VIEWEG, A. SCHLEY and I. A. SCHWARZ, "Polyolefine. Kunststoff-Handbuch IV" (Hanser Verlag, München, 1969).
5. A. TURNER-JONES, J. M. AIZLEWOOD and D. R. BECKETT, *Makromol. Chem.* **75** (1964) 134.
6. G. NATTA and P. CORRADINI, *Atti Accad. Nazl. Lincei* **21** (1956) 365.
7. H. D. KEITH, F. J. PADDEN, N. M. WALTER and H. W. WYCKOFF, *J. Appl. Phys.* **30** (1959) 1485.
8. Z. W. WILCHINSKY, *ibid.* **31** (1960) 1969.
9. F. J. PADDEN and H. D. KEITH, *ibid.* **30** (1959) 1479.
10. J. M. CRISSMAN, *J. Polym. Sci.* **A2** (1969) 398.
11. Y. FUJIWARA, *Colloid Polym. Sci.* **253** (1975) 273.
12. A. J. LOVINGER, J. O. CHUA and C. C. GRYTE, *J. Polym. Sci. Polym. Phys. Ed.* **15** (1977) 641.
13. H. J. LEUGERING, *Makromol. Chem.* **109** (1967) 204.
14. A. TURNER-JONES and A. J. COBBOLD, *Polym. Lett.* **6** (1968) 539.
15. A. DUSWALT, *Amer. Chem. Soc. Div. Org. Coat.* **30** (1970) 93.

16. W. ULLMANN and J. H. WENDORFF, *Progr. Coll. Polym. Sci.* **66** (1979) 25.
17. P. FORGÁCS, B. P. TOLOCHKO and M. A. SHEROMOV, *Polym. Bull.* **6** (1981) 127.
18. K. H. MOOS and B. TIGLER, *Angew. Makromol. Chem.* **94** (1981) 213.
19. K. H MOOS, Dissertation, Darmstadt (1983).
20. K. H. MOOS, and B. J. JUNGNICKEL, *Angew. Makromol. Chem.* **132** (1985) 135.
21. P. JACOBY, B. H. BERSTED, W. J. KISSEL and C. E. SMITH, *J. Polym. Sci.* **B24** (1986) 461.
22. J. GARBARCZYK, and D. PAUKSZTA, *Coll. Polym. Sci.* **263** (1985) 985.
23. *Idem., Polymer* **22** (1981) 562.
24. F. L. BINSBERGEN and B. G. M. de LANGE, *ibid.* **9** (1968) 23.
25. D. R. MORROW, *J. Macromol. Sci. Phys.* **B3** (1969) 53.
26. GUAN-YI SHI, BIN HUANG and JUNG-YUN ZHANG, *Makromol. Chem. Rapid Commun.* **5** (1984) 573.
27. GUI-EN ZHOU, ZHI QUN HE, JIAN-MIN YU and ZWE--WEN HAN, *Makromol. Chem.* **187** (1986) 633.
28. GUAN-YI SHI, BIN HUANG, YOU-HONG COA, HZIQUN HE and ZHE-WEN HAN, *ibid.* **187** (1986) 643.
29. SHI GUANYI, HUANG BIN, ZHING JINGYUN and CAO YOUHONG, *Sci. Sinica, Ser. B* **30** (1987) 225.
30. J. VARGA, *J. Thermal Anal.* **31** (1986) 165.
31. J. VARGA, G. GARZÓ and A. ILLE, *Angew. Makromol. Chem.* **142** (1986) 171.
32. J. VARGA and F. TÓTH, *Makromol. Chem. Makromol. Symp.* **5** (1986) 213.
33. J. VARGA, *J. Thermal Anal.* **35** (1989) 1891.
34. E. J. ADDINK and J. BEINTEMA, *Polymer* **2** (1961) 185.
35. K. D. PAE, D. R. MORROW and J. A. SAUER, *Nature* **211** (1966) 514.
36. J. KARDOS, A. W. CHRISTIANSEN and E. A. BEAR, *J. Polym. Sci. A2* **4** (1966) 777
37. H. AWAYA, *J. Polym. Sci. Polym. Lett.* **4** (1966) 127
38. M. KOJIMA, *J. Polym. Sci. A-2* **6** (1968) 1255.
39. K. D. PAE, *ibid.* **6** (1968) 657.
40. D. R. MORROW and B. A. NEWMAN, *J. Appl. Phys.* **39** (1968) 4944.
41. A. TURNER-JONES, *Polymer* **12** (1971) 487.
42. B. LOTZ, S. GRAFF and J. C. WITTMANN, *J. Polym. Sci. Polym. Phys. Ed.* **24** (1986) 2017.
43. G. NATTA and P. CORRADINI, *Nouvo Cimento Suppl.* **15** (1960) 40.
44. R. L. MILLER, *Polymer* **1** (1960) 135.
45. J. A. GAILEY and R. H. RALSTON, *SPE Trans.* **4** (1964) 29.
46. G. BODOR, M. GRELL and A. KALLÓ, *Faserforsch Textil-Tech.* **15** (1964) 527.
47. P. B. Mć ALLISTER, F. J. CARTER and R. M. HINDE, *J. Polym. Sci. Polym. Phys. Ed.* **16** (1978) 49.
48. P. CORRADINI, C. Dé ROSA, G. GUERRA and V. PETRACCO, *Polymer Commun.* **30** (1989) 281.
49. H. D. KEITH and F. J. PADDEN, *J. Appl. Phys.* **34** (1963) 2409.
50. *Idem., Polymer* **27** (1986) 1463.
51. D. C. BASSETT and A. S. VAUGHAN, *ibid.* **27** (1986) 1472.
52. A. KELLER and J. R. S. WARNING, *J. Polym. Sci.* **17** (1955) 447.
53. D. R. NORTON and A. KELLER, *Polymer* **26** (1985) 704.
54. F. L. BINSBERGEN and B. G. M. de LANGE, *ibid.* **9** (1968) 23.
55. D. C. BASSETT and R. H. OLLEY, *ibid.* **25** (1984) 935.
56. R. H. OLLEY, and D. C. BASSETT, *ibid.* **30** (1989) 399.
57. K. D. HERDT and J. H. KALLWEIT, *Colloid Polym. Sci.* **260** (1982) 413.
58. P. DOBBERT, *Acta Polym.* **41** (1990) 9.
59. J. M. HAUDIN, in "Optical Properties of Polymers", edited by G. H. Meeten (Elsevier Applied Science, London, New York, 1986) Ch. 4.
60. J. VARGA, *Angew. Makromol. Chem.* **104** (1982) 79.
61. M. O. B. IDRISSE, B. CHALBERT and J. GUILLET, *Makromol. Chem.* **186** (1985) 881.
62. B. LOTZ, B. FILLON, A. THERRY and J. C. WITTMANN, *Polym. Bull.* **25** (1991) 101.
63. H. AWAYA, *Polymer* **29** (1988) 591.
64. P. H. GEIL, *J. Appl. Phys.* **33** (1962) 642.
65. R. H. OLLEY, *Sci. Progr. Oxf.* **70** (1986) 17.
66. F. J. KHOURY, *J. Res. Nat. Bur. Stand.* **A70** (1966) 29.
67. J. A. SAUER, D. R. MORROW and G. C. RICHARSON, *J. Appl. Phys.* **30** (1965) 3017.
68. F. J. PADDEN and H. D. KEITH, *J. Appl. Phys.* **44** (1973) 1217.
69. M. KOJIMA, *J. Polym. Sci. A2* **597** (1967) 615.
70. A. J. LOVINGER, *J. Polym. Sci. Polym. Phys. Ed.* **21** (1983) 91.
71. B. LOTZ and J. C. WITTMANN, *ibid.* **24** (1986) 1541.
72. H. SANO, T. USAMI and H. NAKAGAWA, *Polymer* **27** (1986) 1497.
73. M. O. B. IDRISSI, B. CHABERT and J. GUILLET, Makromol. Chem. **187** (1986) 2001.
74. R. J. SAMUELS and R. J. YEE, *J. Polym. Sci. Polym. Phys. Ed. A2* **10** (1972) 385.
75. R. J. SAMUELS, *ibid.* **13** (1975) 1417.
76. J. J. LAURITZEN and J. D. HOFFMAN, *J. Res. Nat. Bur. Stand.* **A64** (1960) 73.
77. J. K. GODOWSKY and G. L. SLONIMSKY, *J. Polym. Sci.* **12** (1974) 1053.
78. M. AVELLA, E. MARTUSCELLI and M. PRACELLA, *J. Thermal Anal.* **28** (1983) 237.
79. H. W. WYCKOFF, *J. Polym. Sci.* **62** (1962) 83.
80. C. De ROSA, G. GUERA, V. PETRACONNE and A. TUZI, *Polymer* **28** (1987) 143.
81. W. R. KRIEGBAUM and J. UEMATSU, J. Polym. Sci. **A3** (1965) 767.
82. V. PETRACCONE, G. GUERRA, C. De ROSA and A. TUZI, *Macromolecules* **18** (1985) 813.
83. K. KAMIDE and K. TOYAMA *Sen-i Gakkaishi* **25** (1969) 49.
84. B. MONASSE and J. M. HAUDIN, *Colloid Polym. Sci.* **263** (1985) 822.
85. J. G. FATOU, *Eur. Polym. J.* **7** (1971) 1057.
86. M. MUCHA, *J. Polym. Sci. Polym. Symp.* **69** (1981) 79.
87. W. W. COX, and A. A. DUSWALT, *Polym. Engng Sci.* **7** (1967) 1.
88. J. VARGA, F. BIRÓ, F. SCHULEK-TÓTH, I. VARGA and J. VOLK, *Müanyag és Gumi* **27** (1990) 133.
89. W. WENIG and K. MAYER, *Colloid Polym. Sci.* **258** (1980) 1009.
90. J. W. TEH, *J. Appl. Polym. Sci.* **28** (1983) 605.
91. A. GALESKI, M. PRACELLA and E. MARTUSCELLI, *J. Polym. Sci. Polym. Phys. Ed.* **22** (1984) 739.
92. P. PRENTICE, *Polymer* **23** (1982) 1189.
93. B. WUNDERLICH, "Macromolecular Physics", Vol. 2 (Academic Press, New York, San Francisco, London, 1976).
94. J. VARGA, Y. FUJIWARA and A. ILLE, *Periodica Polytech. Chem. Engng* **34** (1990) 255
95. J. D. HOFFMAN, G. T. DAVIES and J. J. LAURITZEN, in "Treatise on Solid State Chemistry", edited by N. B. Hanny Vol. 3 (Plenum Press, New York, 1976) Ch. 7
96. E. J. CLARK and J. D. HOFFMAN, *Macromolecules* **17** (1984) 878.
97. G. VIDOTTO, D. LEWY and A. J. KOVÁCS, *Colloid Z.Z. Polym.* **230** (1969) 289.
98. W. BANKS, A. SHARPLES and G. THOMSON, *Eur. Polym. J.* **2** (1966) 309.
99. J. VARGA, G. GARZÓ and P. SMELKÓ, *Magy. Kém. Folyóirat* **95** (1989) 471.
100. J. VARGA, F. SCHULEK-TÓTH and A. ILLE, *Colloid Polym. J.* **269** (1991) 655.
101. H. H. KAUSCH, "Polymer Fracture" (Springer, Berlin, Heidelberg, New York, 1978).
102. K. FRIEDRICH, *Kunststoffe* **69** (1979) 796.
103. T. PAKULA, A. GALEWSKY and E. PIORKOWSKA, *Polym. Bull.* **1** (1979) 275.
104. J. VARGA, *Angew. Makromol. Chem.* **112** (1983) 161.
105. F. LEDNICKY, *Polym. Bull.* **11** (1984) 579.
106. *Idem., Makromol. Chem.* **188** (1987) 619.
107. G. E. SCHULZE and H. P. WILBERT, *Colloid Polym. Sci.* **267** (1989) 108.
108. A. KELLER and J. MANCHIN, *J. Makromol. Sci.* **B1** (1967) 41.

109. A. PETERLIN, in "Structure and Properties of Oriented Polymers", edited by I. M. Ward (Applied Science, London, 1975) pp. 46–8.
110. A. KELLER, in "Ultra-High Modulus Polymers", edited by A. Cifferi and I. M. Ward (Applied Science, London, 1977) Ch. 11.
111. V. A. KARGIN and G. P. ANDRIANOVA, *Dokl. Akad. Nauk SSSR* **146** (1962) 1337.
112. H. J. LEUGERING and G. KIRSCH, *Angew. Makromol. Chem.* **33** (1973) 17.
113. J. VARGA, *ibid.* **112** (1983) 191.
114. A. E. WOODWARD, "Atlas of Polymer Morphology" (Hanser, Münich, Vienna, New York, 1989) Ch. VIII.
115. J. VARGA, *Periodica Polytech. Chem. Engng* **28** (1984) 117.
116. Z. TADMOR, *J. Appl. Polym. Sci.* **18** (1974) 1753.
117. M. R. KANTZ, H. D. NEWMAN and F. H. STIGALE, *ibid.* **16** (1972) 1249.
118. D. R. FITCHUM and Z. MENCIK, *J. Polym. Sci. Polym. Phys. Ed.* **11** (1973) 951.
119. Z. MENCIK and D. R. FITCHMUN, *ibid.* **11** (1973) 973.
120. G. MENGES, A. WÜBKEN and B. HORN, *Colloid Polym. Sci.* **254** (1976) 267.
121. M. FUJIYAMA, H. AWAYA and S. KIMURA, *J. Appl. Polym. Sci.* **21** (1977) 3291.
122. M. FUJIYAMA and K. AZUMA, *ibid.* **23** (1979) 2807.
123. S. S. KATTI and J. M. SCHULTZ, *Polym. Engng Sci.* **22** (1982) 1001.
124. F. ALTENDORFER and H. JANESCHITZ-KRIEGL, *Kunststoffe* **74** (1984) 325.
125. F. ALTENDORFER and E. STEIL, *ibid.* **76** (1986) 47.
126. J. TROTIGNON and J. VERDU, *J. Appl. Polym. Sci.* **34** (1987) 1.
127. *Idem., ibid.* **34** (1987) 19.
128. J. KARGER-KOCSIS and I. CSIKAI, *Polym. Engng Sci.* **27** (1987) 241.
129. J. KOPPELMANN, E. FLEISCHMANN and G. LEITNER, *Rheol. Acta.* **26** (1987) 548.
130. E. FLEISCHMANN and J. KOPPELMANN, *Kunststoffe* **77** (1987) 405.
131. D. G. M. WRIGHT, R. DUNK, D. BOUVART and M. AUTRON, *Polymer* **29** (1988) 793.
132. M. FUJIYAMA, T. WAKINO and I. KAWASAKI, *J. Appl. Polym. Sci.* **35** (1988) 29.
133. A. DIMIAN, G. VILLOUTREIX and R. BERLOT, *Eur. Polym. J.* **24** (1988) 215.
134. J. KARGER-KOCSIS and K. FRIEDRICH, *Int. J. Fatigue* **11** (1989) 161.
135. E. FLEISCHMANN, P. ZIPPER, A. JÁNOSI, W. GEYMAYER, J. KOPPELMANN and J. SCHURZ, *Polym. Engng Sci.* **29** (1989) 835.
136. J. VARGA and G. W. EHRENSTEIN, in "Technologie der Eigenverstarkung von Thermoplasten", edited by G. W. Ehrenstein (Institut Werkstofftechnik Universität-Gesamthochschule Kassel, Kassel, 1987).
137. H. DRAGAUN, H. HUBENY and H. MUSCHIK, *J. Polym. Sci. Polym. Phys. Ed.* **15** (1977) 1779.
138. H. MUSCHIK, H. DRAGAUN and P. SKALICKY, *Progr. Colloid Polym. Sci.* **64** (1978) 139.
139. H. MUSCHIK and H. DRAGAUN, *ibid.* **66** (1979) 319.
140. J. VARGA, unpublished results.
141. H. POTENTE, *Kunststoffe* **67** (1977) 98.
142. G. N. KORAB, W. D. GRINJUK and O. J. WESELOW, *ZIS Mitteil.* **7** (1982) 734.
143. V. HORN, *Schweisstechnik* **33** (1983) 268.
144. G. W. EHRENSTEIN and U. EGEN, *Kunststoffberater* **29** (7–8) (1984) 15.
145. M. J. OLIVEIRA and D. A. HEMSLEY, *Br. Polym. J.* **17** (1985) 269.
146. U. EGEN and G. W. EHRENSTEIN, *Plastverarbeiter* **37** (11) (1986) 61.
147. U. EGEN, Dissertation, Universität-GH, Kassel, 1985. (Deutsche-Verlag Für Schweisstechnik, 1986).
148. H. MUSCHIK, M. RADAX, H. DRAGAUN and F. EICHINGER, *Kunststoffe* **76** (1986) 346.
149. L. I. BEZRUK, G. B. ESAULENKO, G. N. KORAB and N. A. USKOV, *Dokl. Akad. Nauk SSSR* **286** (1986) 1151.
150. H. MUSCHIK and H. DRAGAUN, *Angew. Makromol. Chem.* **158/159** (1988) 363.
151. G. W. EHRENSTEIN and A. K. SCHLARB, *Kunststoffe* **78** (1988) 541.
152. G. W. EHRENSTEIN, A. K. SCHLARB and J. VARGA, *Müanyag és Gumi* **25** (1988) 339.
153. A. K. H. SCHLARB, Dissertation, Universitat-GH Kassel, 1989 (Ehrenstein, Kassel, 1989).
154. H. POTENTE, P. MICHEL and B. RUTHMANN, *Kunststoffe* **77** (1987) 711.

Received 2 September
and accepted 10 September 1991